Design and Fabrication of a Thin Film Optogenetic ECoG Array with Individually Addressable μLEDs

Medha Krishnaswamy

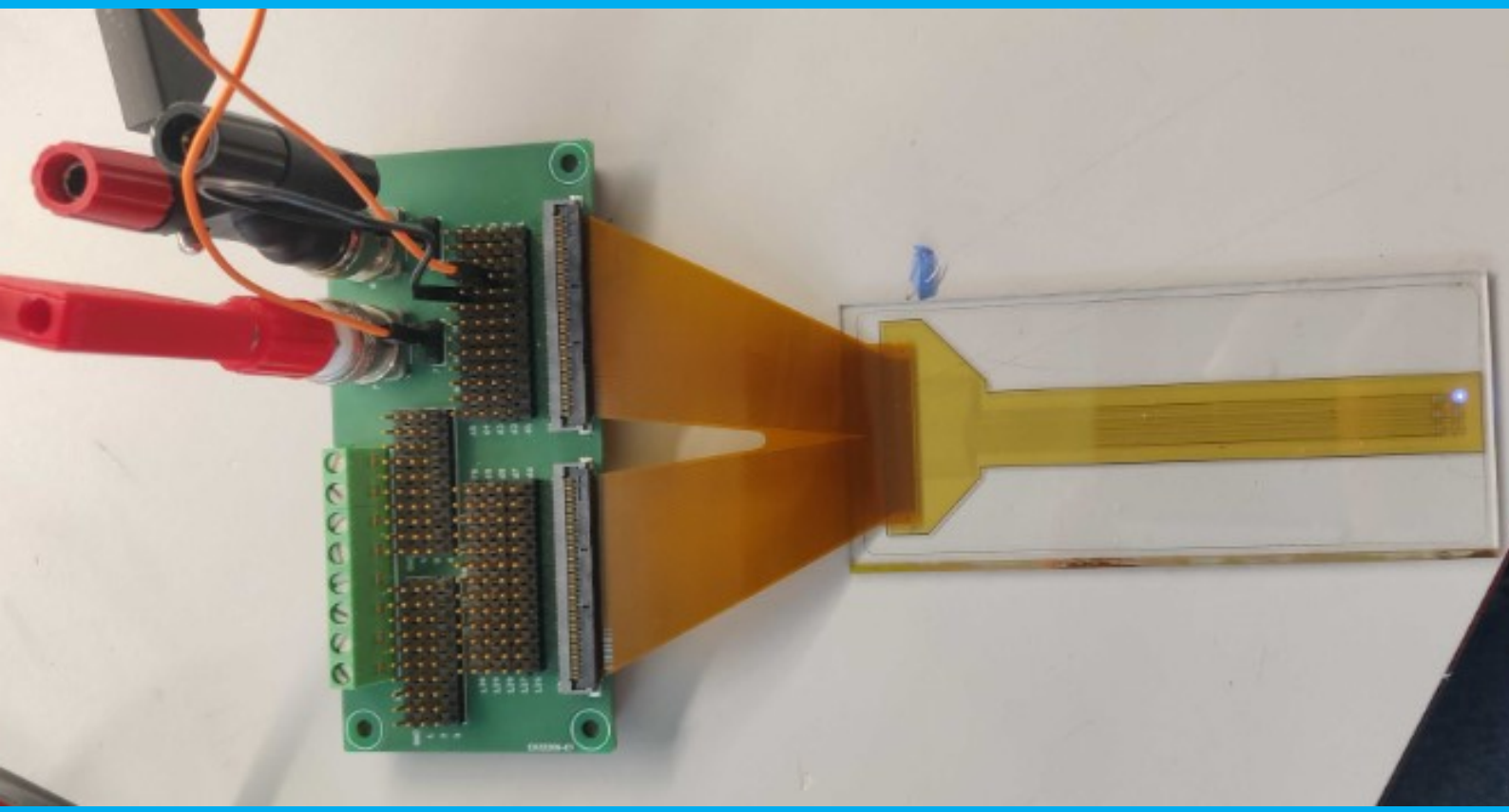

Design and Fabrication of a Thin Film Optogenetic ECoG Array with Individually Addressable μLEDs

By

Medha Krishnaswamy

in partial fulfilment of the requirements for the degree of

Master of Science
in Biomedical Engineering
Specialization: Medical Devices and Bioelectronics

at the Delft University of Technology,
to be defended publicly on Friday October 29, 2021 at 2:00 PM.

Project duration:	March 1, 2021 – October 29, 2021	
Supervisor:	Prof. Dr. Vasiliki Giagka,	TU Delft
	Ronaldo Martins da Ponte,	TU Delft
Thesis committee:	Prof. Dr. Wouter Serdijn,	TU Delft
	Prof. Dr. Massimo Mastrangeli,	TU Delft
	Dr. Auke Kronemeijer,	Holst Centre

Abstract

Optogenetics is a neuromodulation technique that uses light to control genetically modified cells to express light sensitive ion channels. Optogenetics allows stimulation of only the specific cells in the region that have been genetically modified and thus results in a high resolution of stimulation.
Currently optogenetic implants are used to stimulate specific regions in the brain, either deep in the cortex or on certain regions on the surface of the cortex. An implant with a larger surface area would potentially allow stimulation of the entire cortex simultaneously, if required. By also including recording sites on this implant, it is possible to record responses at one end of the brain produced due to optogenetic stimulation on the other end of the brain. Thus, the underlying neural circuit can be mapped for investigation.
Thin film technology (TFT) so far has had a huge impact in the field of large flexible displays. The flexible substrates and processes employed for the fabrication of flexible displays can be used for the realisation of an optogenetic array that covers the cortex of the brain while being flexible and conformal to the shape of the brain.
This work explores the implementation of TFT in fabricating a flexible large area high-density optogenetic ECoG array. The fabricated array features multi-stacked alternate layers of thin film Au/Ti (for electrodes and interconnects) and thin film SiN (insulation and passivation) on a flexible polyimide substrate to provide a high-density array for improved resolution. Commercial μLEDs were bonded to the surface of the array using ICA (Isotropic Conducting Adhesive) to provide on-site stimulation. The resulting flexible implant was characterised to determine the electrode impedance, behaviour of the passivation layer in phosphate buffered saline and thermal characteristics of the μLEDs. The final device was implanted on the cortex of a mouse.

Acknowledgement

I would like to express my hearty gratitude to all the people who have contributed to my growth as a researcher as well as an individual during the last year.
First of all, I would like to thank Vasso for giving me the opportunity to be a part of the Bioelectronics group to pursue my MSc thesis. Although I was stressed and confused the innumerable times I approached you with questions, your calm and cheery demeanour while guiding me to find my own answers really motivated me to keep up with my work. Especially during the past year when we were all so isolated, it was refreshing to speak to you on our weekly meetings!
I am also grateful to Auke for providing me the opportunity to do my thesis at Holst Centre. The moments where I got overly creative with a lot of different approaches or suggestion, he ensured that I kept on to the right track needed for my thesis.
I would also like to thank Ronaldo, who as my daily supervisor really went above and beyond when it came to helping me with writing the report. His suggestions and his way of explaining concepts using mental exercises to my multitude of doubts during meetings, that would always run a little too long, has truly made all the difference in this journey.
I also extend my gratitude towards Wouter and people from the Bioelectronics group for being so helpful and friendly, allowing me to approach anybody easily for suggestions.
The fabrication and experiments were performed at Holst Centre cleanrooms where I was mentored by Roy Verbeek who helped me to get familiar with microfabrication processes and gave me a lot of useful feedback. I would also like to thank all the engineers in the labs for assisting me during the fabrication process.
During my time at Delft, I also became good friends with Christiaan, Jia-Jun and Mukil without whom I would have found it very hard to keep going in the last year. Thanks for all the great memories!
Finally to my parents for their unconditional love and support, for believing in me and proof-reading my half-written drafts of the report, thank you for the sacrifices so that I could make it this far.

Medha Krishnaswamy
Delft, October 2021

Contents

Abstract iii

Acknowledgement v

List of Figures ix

List of Tables xi

List of Abbreviations xiii

1 Introduction 1
- 1.1 Optogenetics . . . 1
- 1.2 Optogenetic Stimulation with Electrophysiological recording . . . 2
  - 1.2.1 High-Density ECoG recording in Large Areas . . . 3
- 1.3 Thin Film Technology at Holst Centre . . . 3
- 1.4 Aim of the project . . . 4

2 Literature Overview 5
- 2.1 Implementation of Flexible Substrates in Neuromodulation Arrays . . . 5
- 2.2 System Integration of Light Sources on Flexible Substrate . . . 6
- 2.3 Electrophysiological Recording Following Optogenetic Stimulation . . . 7
- 2.4 Thin Film Technology in Optogenetics . . . 9
- 2.5 Chapter Conclusion . . . 10

3 Methods 11
- 3.1 Design of Flexible Large Area Optogenetic Array . . . 11
  - 3.1.1 Shape and space considerations of Optogenetic Array in Mouse Cortex . . . 11
  - 3.1.2 Arrangement of recording and stimulation sites on the Array . . . 13
  - 3.1.3 Routing Considerations for I/O lines on the Array . . . 13
- 3.2 Fabrication of Flexible Large Area Optogenetic Array . . . 15
  - 3.2.1 Au/Ti Sputtering and Etching . . . 16
  - 3.2.2 SiN Deposition and Introduction of Vias . . . 16
  - 3.2.3 System Integration . . . 18
- 3.3 Characterisation Methods . . . 18
  - 3.3.1 Electrochemical Impedance Spectroscopy . . . 18
  - 3.3.2 Characterisation in Phosphate Buffered Saline . . . 18
  - 3.3.3 Thermal Characterisation . . . 19

4 Results and Discussion 21
- 4.1 Microfabrication . . . 21
  - 4.1.1 Au/Ti Layers . . . 21
  - 4.1.2 SiN Deposition and Vias . . . 21
  - 4.1.3 Lasering of Glass and PI . . . 23
- 4.2 Wet Characterisation . . . 23
  - 4.2.1 Electrochemical Impedance Spectroscopy . . . 23
  - 4.2.2 Characterisation of Passivation Layer . . . 24
- 4.3 μLED Bonding . . . 25
- 4.4 Thermal Characterisation . . . 26
- 4.5 Placement of Optogenetic Array on Mouse Cortex . . . 28

5 Conclusion 31
6 Future Work 33
A Arduino Code 35
Bibliography 37

List of Figures

1.1 Channelrhodopsin-2 (ChR2) and halorhodopsin (NpHR) are light-sensitive proteins used in optogenetic studies[33] . . . 1
1.2 Depiction of electrophysiological recording platforms in relation with the anatomy and the area under measurement [27] . . . 2
1.3 Electrophysiological recording methodologies shown here from left to right with EEG as the least invasive and extracellular as the most invasive; the signal fidelity simultaneously increases from EEG to ECoG to extracellular recording . . . 2
1.4 Flexible active matrix OLED on PI [42] . . . 4

2.1 Young's modulus on a log scale of brain tissue and flexible materials, with silicon as the stiffest common substrate [32] . . . 6
2.2 Transfer Printing of μLEDs [32] . . . 7
2.3 Thin Film Deposition and Sputtering shown side by side [32] . . . 8
2.4 Photolithography [32] . . . 8
2.5 OLED array on a parylene-c substrate of 2 μm thickness [23] . . . 9

3.1 Proposed device design with ZIF flex connector . . . 12
3.2 A mouse brain with reference points for Primary Motor Cortex (M1), Somatosensory Cortex (S1) and Visual Cortex (V1) . . . 12
3.3 Initial designs of array with rectangular and circular shapes . . . 13
3.4 Rectangular optogenetic array with electrodes and μLEDs separated by a pitch of 300μm . . . 14
3.5 Rectangular optogenetic array with fewer electrodes and μLEDs for routing . . . 14
3.6 Optogenetic array with two metallization layers separated by a dielectric . . . 15
3.7 Topography of the flexible optogenetic array with various layers of thin films . . . 15
3.8 Design of the 6 inch glass wafer with 4 optogenetic arrays . . . 16
3.8 Processing steps for the fabrication of the first Au/Ti layer . . . 17
3.9 Processing steps for the fabrication of vias on the SiN . . . 17
3.10 Ionic Composition of ECF and PBS [4] . . . 18

4.1 Au interconnects showing overetching In (a), three interconnects of 15 μm width with signs of overetching on the edges is shown. In (b), a maginified image of one of the interconnects with clear overetching on the edges . . . 21
4.2 First Layer of Au/Ti on PI. In (a), the entire array is shown. In (b), a magnified image of the array with the anode and cathode connections for the LED is shown. . . . 22
4.3 Au/Ti interconnect showing vias on SiN larger than conceived with bite-shaped edges at the junction of Au/Ti . . . 22
4.4 Magnified image showing (a) anode and cathode connection for the LED with vias and an electrode on the right and (b) anode with patterned vias after final layer of SiN deposition and patterning . . . 22
4.5 Post lasering of the PI in which (a) shows interconnects being damaged due to error in design and (b) shows a good lasered PI substrate on glass . . . 23
4.6 Schematic for EIS measurement indicating equivalent circuit models . . . 23
4.7 Results for EIS of Au electrodes . . . 24
4.8 (a) Top view of the area considered under the profilometer and (b) Front view of the profile under consideration . . . 24
4.9 Sample Optogenetic Array with a ZIF connector connected to a PCB for LED driving . . . 25
4.10 Microscope images of Optogenetic Arrays with μLEDs bonded to PI where (a) is Sample 4 and (b) is Sample 3 indicating the function μLEDs in red . . . 26
4.11 μLEDs under X-ray showing good contacts with the underlying array . . . 26

4.12 Experimental Setup for Thermal Characterisation is shown in (a) where the Box Lined with Aluminium Foil holds the Arduino, Breadboard and the Optogenetic Array Connected to the PCB and in (b) where the Connections from the Arduino (green arrow) to the Potentiometer (red arrow) and the Optogenetic Array (yellow arrow) can be seen clearly 27
4.13 Graph depicting temperature increase with increase in applied voltage and duty cycle 28
4.14 Tissue responses to temperature increase (Left) and heating factors that cause temperature increase (Right) [10] 28
4.15 Device Design with Space Consideration for Lasering of PI 29
4.16 Final Shape of Array Before Placement on Mouse Cortex 29
4.17 Thin Film Optogenetic Array Placed on the Cortex of a dead Mouse. Disclaimer: The array was fitted on the cortex of an already deceased mouse that was killed after use in a separate experiment performed at the Erasmus MC, for which official permission through the necessary channels in The Netherlands was obtained. 29
4.18 Irregular Topography of the Array due to the presence of 50 μm thick μLEDs 30

List of Tables

4.1 Change in height of SiN before and after 1 week soak in PBS measured using profilometer 25
4.2 Sample Optogenetic Array with a ZIF connector connected to a PCB for μLED driving 25

List of Abbreviations

Anisotropic Conductive Films	ACF
Channelrhodopsin-2	ChR2
Chromium	Cr
Deionised Water	DI
Electrochemical Impedance Spectroscopy	EIS
Electrocorticography	ECoG
Electroencephalogram	EEG
Extracellular Fluid	ECF
Food and Drug Administration	FDA
Galium Nitride	GaN
Gold	Au
Halorhodopsin	NpHR
Hexamethyldisilazane	HMDS
Indium Galium Zinc Oxide	IGZO
Indium Tin Oxide	ITO
Isotropic Conductive Adhesives	ICA
Micro-Light Emitting Diodes	μLEDs
Multielectrode Array	MEA
Organic Light Emitting Diodes	OLED
Plasma-Enhanced Chemical Vapor Deposition	PECVD
Philips Innovation Labs	PInS
Phosphate Buffered Saline	PBS
Platinum	Pt
Polyethylene Naphthalate	PEN
Polyethylenterephthalat	PET
Polydimethylsiloxane	PDMS
Polyimide	PI
Reactive Ion Etch	RIE
Silicon Carbide	SiC
Silicon Nitride	SiN
Tetrafluormethane	CF_4
Thin-Film Technology	TFT
Zero Insertion Force	ZIF

1 Introduction

1.1. Optogenetics

Optogenetics is a neuromodulation technique that is used to activate or inhibit a group of genetically modified neurons using light. Optogenetics allows for the high specificity of the target area as it only allows cells that are genetically modified to be receptive to light to react to the applied stimulation [8]. The advent of optogenetics came with the discovery by microbiologists who observed that the proteins in algae called 'microbial opsins' would open or close ion channels on the application of light of a particular wavelength almost 50 years ago [8, 35]. This behaviour is similar to how neurons open their channels when they are ready to fire signals. By introducing a viral carrier with a microbial protein, it is possible to activate the specific neurons that express the protein [5]. Channelrhodopsin-2 (ChR2) belongs to a family of opsins that is sensitive to blue light (~470 nm); halorhodopsin (NpHR), to yellow (~570 nm) - Figure 1.1. Both ChR2 and NpHR respond to light with milli-second scale blue and yellow pulses, indicating high temporal precision [51].

It is possible to stimulate these genetically modified neurons to depolarise or hyperpolarise by varying the

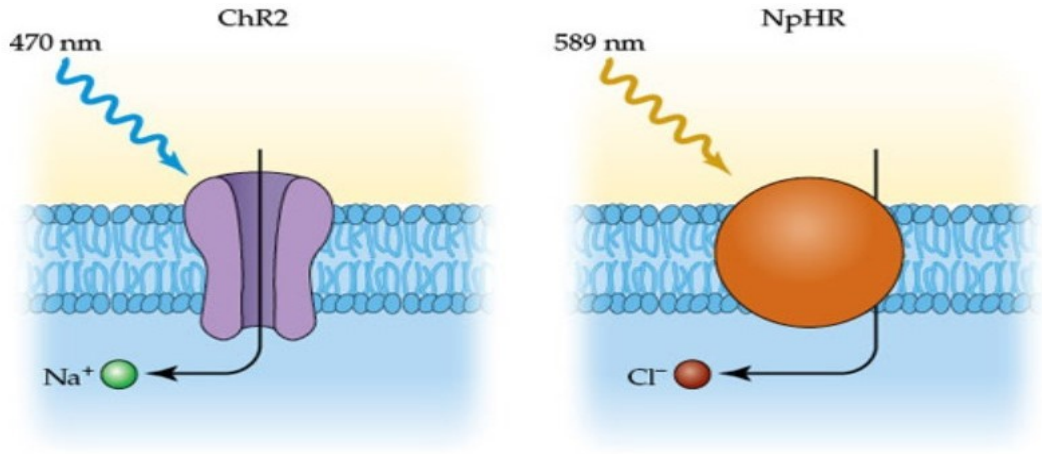

Figure 1.1: Channelrhodopsin-2 (ChR2) and halorhodopsin (NpHR) are light-sensitive proteins used in optogenetic studies[33]

wavelength of light, achieving high specificity and high temporal precision in stimulation. Depending on the application, light sources commonly employed to implement stimulation are lasers or LEDs [5]. Optical fibers and waveguides are commonly used to guide these light sources to specific regions to improve resolution and provide localised stimulation. Opsins such as ChR2 require a minimum 1 mW/mm^2 or more for depolarization. Lasers provide a high collimated beam of light with an optical fiber which can be focused into deep brain structures. The divergence of this light beam increases as the numerical aperture of the optical fiber increases. Optical fibers with diameters less than 50 μm allow point illumination of the target area with high spatial resolution [50].

LEDs provide highly divergent light beams and need to be collimated using optical fibers to achieve suitable stimulation intensity, but coupling with optical fibers reduces the efficiency of stimulation due to coupling

and transmission losses. LEDs provide lower light intensity at the same wavelength as lasers [24]. Lasers and LEDs coupled with optical fibers are still tethered light sources which limit natural movement of the subject during prolonged studies μLEDs on arrays or probes are placed directly on the region being stimulated due to their small sizes, thus reducing the effect of coupling losses with optical fibers. μLEDs are also an attractive option because of their low cost.

1.2. Optogenetic Stimulation with Electrophysiological recording

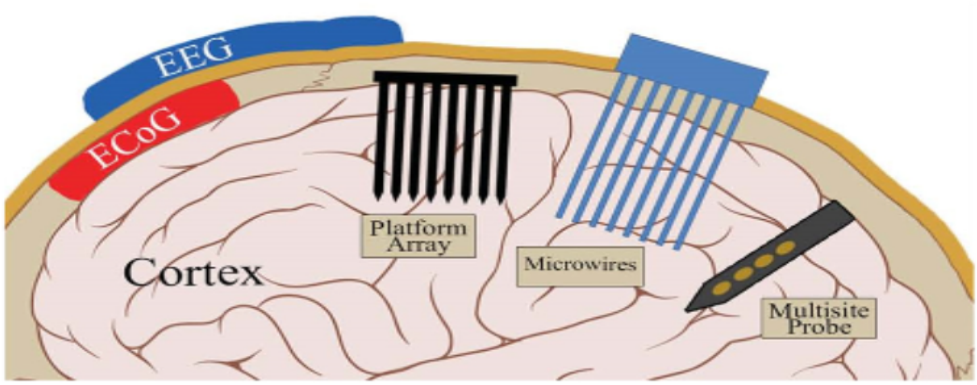

Figure 1.2: Depiction of electrophysiological recording platforms in relation with the anatomy and the area under measurement [27]

Following optogenetic stimulation, it is important to record the responses from the stimulated area. Electrophysiological recording of the brain allows for diagnostic mapping of the area of interest by employing different recording methodologies based on the location of the electrode on the brain. EEG provides information about the total synchronous activity of the neuronal population in the cortex while being the least invasive option, making it a widely used course of action in neuroscience. EEG allows mapping of external electrical activity from large areas of the brain. The signals measured with EEG suffer from the filtering effect of the skull, the signal-to-noise ratio is relatively low and, the recorded signal show low spatial and temporal precision [26, 28]

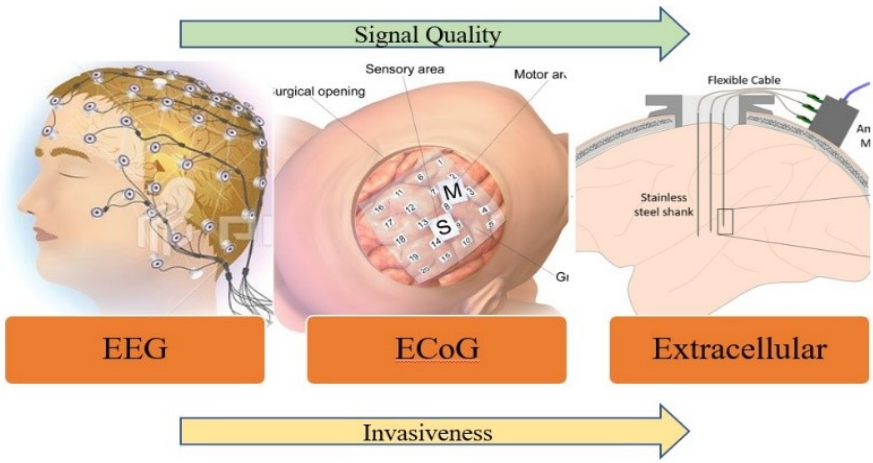

Figure 1.3: Electrophysiological recording methodologies shown here from left to right with EEG as the least invasive and extracellular as the most invasive; the signal fidelity simultaneously increases from EEG to ECoG to extracellular recording

Extracellular recordings obtained from penetrating probes require close contact of the implant with the brain tissue, relatively justifying it as the most invasive. Extracellular recording provides information about action potentials generated from a single or group of neurons from electrodes implanted into the brain's cortex. Implantation of these penetrating electrodes for extracellular recording almost always requires highly

invasive surgery. The penetrating probe, a foreign body, inserted into the brain poses potential issues for both the brain and the probe. Initial problems ranging from immediate foreign body response following implantation to inflammation at the site of implantation occurring from micromotion of the rigid probe due to constant pulsing of the brain. This also affects implant durability leading to delamination of the encapsulation and corrosion of the tracks and electrodes on the probe [27].
Electrocorticogram (EcoG) lies in between both EEG and extracellular recording in terms of invasiveness. ECoG recordings originate from electrodes placed on the cortical surface of the brain. Placement of ECoG is on the brain's cortex, so the challenge faced due to the filtering effect of the skull in EEG recording is avoided. ECoG also reduces the invasiveness of the implant that is introduced by extracellular recording by avoiding the insertion of electrodes into the cortex, thus preventing possible haemorrhage and inflammatory tissue responses due to the inability of rigid electrodes to bend and move as the brain pulses [26, 47]. However, in both ECoG and extracellular recordings, the focus on the properties of the material used for the implant is important because of the interactions that exist between the brain and the implanted device. By moving away from rigid devices to devices with flexible substrates allows a conformal contact of the electrodes to the brain. For extracellular recording devices, flexible substrates make handling difficult during insertion, thus requiring the use of addition equipment to support implantation.

1.2.1. High-Density ECoG recording in Large Areas

The purpose of having an array with a larger surface area is to ensure that responses at one end of the brain to stimulation in another end of the brain is recorded with reduced losses. An array covering a large area also considers the variability in the location of brain functions in different subjects which is shown to be around 5 mm [47].
In present-day clinical diagnosis and treatments, the electrodes used are large(~3 mm diameter), with even larger interspacing between them(~10 mm) to cover a sizeable area on the brain, making it an arduous process to localise the origin of signals due to poor resolution [47]. By incorporating large number of electrodes in relatively small areas, a high-density ECoG array allows the mapping of large regions of the brain surface with high resolution. One option could be to reduce the inter-electrode spacing and increase the number of recording sites, although there exists the complication about connecting a vast number of wires within the small intracranial space available. Introduction of additional layers on a single substrate can provide more space for the interconnects, but the use of common bulk microfabrication techniques limits this solution with an increase in the thickness of the implant.
While increasing the number of recording sites improves the resolution, it is necessary to develop ECoG arrays that accomplish recording in the absence of inflammatory tissue responses and insertion damage. It is therefore vital to consider a substrate with a Young's Modulus that is close to the Young's Modulus of the brain such that it conforms to the shape of the area it is placed on. Such a design consideration will allow signal quality to remain stable over extended periods as the array moves undisturbed with the brain's movement.
Another consideration in optogenetic implants is the position of the recording sites on the implant. Electrodes arranged in densely packed opaque substrates are used to record the responses from the optical stimulation sites, but this reduces the efficiency of light transmitted through the electrode arrangement. The use of transparent electrode materials, such as graphene and ITO (Indium Tin Oxide), have been implemented to increase light transmission and efficiency of the stimulation in such scenarios[29, 46].

1.3. Thin Film Technology at Holst Centre

Holst Centre, an innovation and research centre in Eindhoven, The Netherlands have been using thin film technology for accomplishing deposition and patterning techniques to fabricate thin-film transistors for flexible displays, thin film photovoltaics and OLED applications. The use of these fabrication techniques allow for realisation of extremely flexible end products that shift away from the conventional rigid structures. This flexibility comes from the use of substrates such as polyethylene naphthalate (PEN) or polyimide (PI).
These flexible substrates can be used for the realisation of an optogenetic array that covers the cortex of the brain while being flexible and conformal to the shape of the brain. Holst Centre has used PI as substrate for flexible OLED imagers with IGZO thin-film transistor backplanes [42]. These thin-film transistors have been used in active matrices to deliver high resolution displays.
A large electrode array with high resolution can be implemented with fewer mask layers than a thin-film transistor backplane. Also, the use of a maskless lithography tool at Holst Centre which uses laser to pattern structures on metals and open vias on passivation layers facilitates the implementation of an optogenetic

Figure 1.4: Flexible active matrix OLED on PI [42]

array with multiple layers of metal easier.

1.4. Aim of the project

The discussion so far has been about the need for an optogenetic implant which also facilitates recording of the evoked potentials using electrophysiological recording techniques. An increase in the number of stimulation sites and rearrangement of the recording points on a flexible substrate in the design, could result in an improvement of stimulation efficiency. A large number of untethered stimulation sites also allow for multi-point stimulation of the cortex, thus allowing high-resolution of stimulation. This increase in the number of stimulation sites also requires a similar increase in the number of recording points (electrodes) to map the responses in high resolution. The problem to circumvent here is to design such a flexible array using Holst Centre's thin film technology while making space for the considerable number of wires that will result from the stimulation and recording sites in the available space.
Since most initial testing of in-vivo implants calls for animal testing, the first device design will seek to implement the possibilities of the implant on the cortex of a mouse's brain. It is also crucial to understand if the processes employed during fabrication with thin film technology allow for the development of an optogenetic array that is compatible with the biological environment of the mouse's brain.
For the implementation of this project, the utilisation of the mouse as the animal model helps formulate the problem statement as follows: can thin film technology be used to fabricate a flexible, large area and high density optogenetic ECoG array to be implanted in the cerebral cortex of a mouse? If so, is the process employed to fabricate the array suitable for an optogenetic implant? What are the characterisation methods that could be used to investigate the fabrication process?
This project, aims to implement a flexible large area high-density optogenetic ECoG array using the thin film technology available at Holst Centre and characterise it.

2

Literature Overview

The realisation of a flexible, large area and high-density optogenetic ECoG array as discussed in Chapter 1 can be made possible by looking into other published works to gain an insight into the existing materials used for flexible substrates, the methods used for integration of LEDs onto the flexible substrates, and the processes for electrode fabrication for electrophysiological recording following stimulation.

2.1. Implementation of Flexible Substrates in Neuromodulation Arrays

Optogenetic stimulation using an array of LEDs requires the placement of the implant on the surface of the brain. This direct contact of foreign material on the brain evidently results in numerous reactions and responses by the body. However, the first observation upon placement of an implant is how it sits on the surface of the brain. As the Young's Modulus of the brain's soft tissue is around 0.5 to 2 kPa [44], an implant with a rigid substrate offers a higher Young's Modulus, like that of thin-film silicon (~4.7 GPa), and micromotion of the implant would cause abrasions and tissue damage as the brain flexes and contracts [14]. Substrate materials have to be chosen such that the reaction after implantation is minimised. An implant with a flexible substrate such as PDMS has a much lower Young's Modulus (~100 kPa to 3 MPa) [30], which makes it conformal to the shape of the brain and thus, moves with the brain. The conformal contact provided by a flexible implant also allows for efficient stimulation.

So, for a flexible substrate to be employed for an optogenetic implant, it should have a Young's Modulus sufficiently closer to that of the brain while also survive the process of μLED integration and electrode deposition onto its surface. The substrate material should indicate good biocompatibility and not cause extreme foreign body response, survive in saline environments without a high rate of dissolution or cracking.

Commonly used flexible materials as substrates so far have been polymer-based, from Polyimide [21, 38], PDMS [26, 45], Parylene-C [25] to SU-8 [53]. Based on the application and functionality required, these different materials provide unique advantages to the overall implant. For example, parylene-C was used as a substrate by Hara et al. [13] for carrying platinum electrodes to be placed on the surface of a rat's M1 cortex for in-vivo neural recording. The parylene substrate, along with a parylene encapsulation was shown to survive for a maximum of 12 months in-vivo with little to no change in the EIS measurements indicating that the electrodes were well protected during the study duration [13]. Parylene was chosen for its low Young's Modulus to prevent a mechanical mismatch with the rat brain. The observed 60% transparency of parylene-C [20] for blue light (~470 nm wavelength) also makes it an ideal candidate for an optogenetic implant, as it allows integration of light sources on its surface, preventing direct contact of the heated μLEDs with the brain tissue. This method, adopted by Kwon et al. [26], used a parylene/metal/parylene technique for fabrication of the electrode array and an array of LEDs separated from a PDMS stamp was bonded using SU-8 to the electrode array. This design of light transmittance through the parylene-C curbed the temperature increase in the region surrounding the device to 0.1 °C at a minimum driving voltage of 2.7 V at the expense of the intensity of the μLEDs being reduced to 60% [26].

SU-8 is also another flexible polymer that is commonly used as a negative photoresist in standard lithography processes. It is a hard cross-linked polymer that is used either as a substrate or device layer based on the application. SU-8 as a substrate has a high tensile strength [37], and is hence sturdy even when reduced to submicron thicknesses. This can be observed in an extremely flexible microelectrode array designed by

Zhao et al. [52] which can be wrapped around a probe to be inserted into a mouse's brain. The SU-8 was spin-coated onto a silicon substrate with a nickel metal release layer between the SU-8 and the silicon. This entire implant was less than 1 μm thick after separating from the silicon in a nickel etchant and remained functional in-vivo for almost 4 months [52]. This high tensile strength and biocompatibility of SU-8 however are not enough as thin-film SU-8 substrates have shown to be susceptible to crack formation in long-term animal experiments in several works [7, 9].
Similarly, PDMS is another polymer material with low Young's Modulus and high stretchability, but its porous structure and hydrophobic tendencies absorb water leading to the generation of micro-cracks on the substrate [32]. Parylene, because of its low water absorption, has been used to fill in the pores in PDMS substrates, to reduce the water absorption and increase the longevity of the implant in multielectrode arrays of parylene-caulked PDMS substrate [19]. In a PDMS based gold multielectrode array (MEA) designed by Biswas et al. [2], the mismatch of the thermal coefficient of expansion between PDMS ($20x10^5 K^{-1}$) and gold ($14.2x10^6 K^{-1}$) caused the formation of buckles on the PDMS substrate after fabrication [2].
Polyimide (PI), another commercially available polymer, though not FDA (Food and Drug Administration) approved, has been used and tested as substrates in the form of PI2611 (also called BPDA/PPD) for a large number of neural MEAs. Although the Young's Modulus of PI (2.5 GPa) is higher than PDMS, this makes it easier for handling while implantation. A 5 μm PI as a substrate implemented by Stieglitz [43] involves a double-sided electrode array for stimulation and recording of nerves. The 4 layers of PI alternating between the metallization layers of titanium and platinum served as both substrate and insulation layer for the implant with reactive ion etching (RIE) being used to open the electrode sites on the front and back of the PI [43]. The processing of PI is also very similar to common microelectronic processes, thereby reducing production costs, and allowing high repeatability. This can be observed in an intracortical electrode array designed by Rousche et al. [38] where standard photolithography methods were used to surface micromachine PI and gold/chromium layers on silicon wafers. The PI surface chemistry is shown to be modified with vias of 40 μm for bioactive species to bond on the surface to improve tissue integration and longevity of the implant. It was subsequently implanted in rats, however, no information was provided on the long-term functioning of the PI in the implant[38].

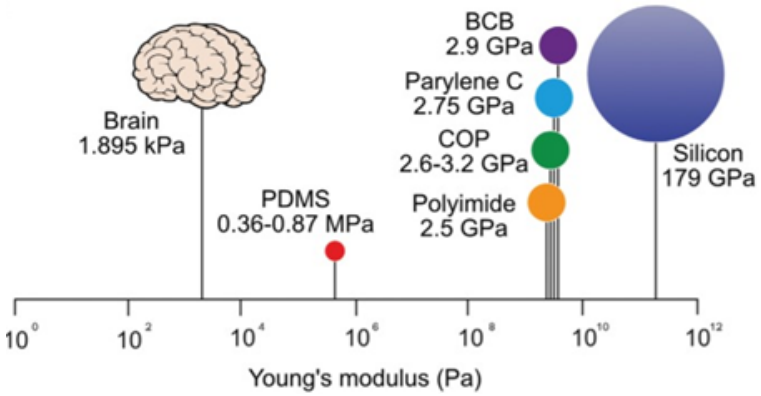

Figure 2.1: Young's modulus on a log scale of brain tissue and flexible materials, with silicon as the stiffest common substrate [32]

2.2. System Integration of Light Sources on Flexible Substrate

μLEDs when used as light sources in optogenetic implants need to be integrated into the chosen flexible substrate. A commonly used μLED type are the GaN-based μLEDs. These μLEDs can be either grown on the surface of a substrate [48], transfer printed from one substrate to another using laser lift-off [17] or hybrid integrated on a substrate of choice using commercial μLEDs [1, 26]. However, GaN-based μLEDs that are grown can be grown only on SiC or sapphire wafers, not only is the process expensive, it allows for little flexibility in processing as μLEDs of only one wavelength can be grown on a substrate. To increase the choice of substrates, Wu et al. [48] grew μLEDs on a silicon substrate with quantum well epitaxial layers grown on it to have a 460 nm wavelength for blue light illumination. The μLED structures were plasma etched and the final device showed high spatial resolution with tunable illumination of the μLEDs[48]. Though silicon provided

better heat dissipation compared to sapphire or SiC, all the substrates used are rigid.
For the integration of μLEDs onto flexible substrates, transfer printing of the μLEDs grown on rigid substrates can be considered. Jeong et al. [18] designed an optofluidic system where GaN μILEDs (inorganic light-emitting diodes) grown on a sapphire wafer were separated from the substrate by inductively coupled plasma RIE for etching of the GaN, followed by laser lift-off of the μILEDs from the sapphire[18]. Laser lift-off uses the high-intensity light from the laser to dissociate the GaN into gallium and nitride, which turns the gallium liquid and allows for the nitride to be separated from the sapphire wafer. The μILEDs were then transferred to PDMS stamps to be used to transfer the μILEDs onto a PET film for optical stimulation. Laser lift-off benefits from being able to choose a substrate for a specific application, facilitating thin-film μLEDs, as sapphire is a difficult material to micromachine below 100 μm [31].
This similar use of a PDMS stamp for transferring commercial μLEDs to a parylene-C substrate was used by

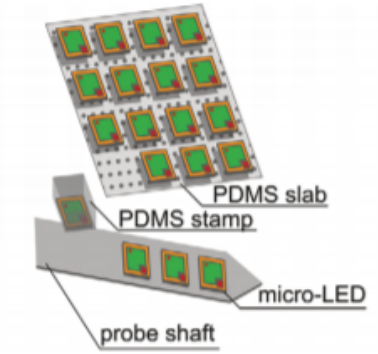

Figure 2.2: Transfer Printing of μLEDs [32]

Kwon et al. [26] to design a hybrid opto-ECoG array. However, since there was no need for separation from an already grown sapphire or SiC wafer, the entire process was much simpler. The substrate was aligned with the PDMS stamp and the μLEDs were separated when the PDMS stamp was heated to 90°C [26]. The use of commercial μLEDs also allows a combination of different wavelengths of light to be used for either stimulation or inhibition in one implant.
To maximise light transmission through the flexible substrates, μLEDs are integrated with the light-emitting surface facing vias (holes) created in the substrate. This was done by Ji et al. [21] in their opto-electric neural interface by photoetching through a 50 μm thick SU-8 layer and a 5 μm PI layer at the bottom. The μLEDs are placed one by one with their contact ends facing the top to allow for wire bonding with the gold contacts and a UV curable adhesive is applied around the SU-8 wells to firmly adhere the μLEDs[21].
Most optogenetic implants discussed so far have both μLEDs for stimulation and electrodes for recording the responses from the cells, however, the increase in the number of components on the substrates makes it difficult to connect multiple wires and interconnections. The loss of stiffness that comes with these flexible substrates makes it difficult for conventional wire bonding techniques to be implemented. The use of an alternative connection method, such as Anisotropic Conduction Films (ACF), which utilizes lead-free bonding materials making it less toxic, can be used to bond the μLEDs to the flexible substrate.

2.3. Electrophysiological Recording Following Optogenetic Stimulation

Following stimulation of the targeted region in the brain, it is necessary to have some form of readout of the neural activity induced. A combination of optogenetic stimulation with electrophysiological recording will therefore allow the measurement of neural activity. Electrode arrays can be patterned on the optogenetic implant to simultaneously stimulate and record the responses with no delay in the electrophysiological recording.
Based on the application, the size and material of the electrodes can be varied, however, care should be taken to ensure that the electrode material is not toxic or induce cytotoxicity in the brain. Careful selection of materials increases biocompatibility, longevity and recording quality of the device. During recording, around the electrode/electrolyte boundaries, faradaic and capacitive (double-layer charging) reactions occur, that affect the chemistry of the electrode over time. The design of electrodes has to consider these factors along with the electrochemical impedance of the electrode material.
Commonly used electrode materials are gold, platinum, titanium, ITO (indium tin oxide) and recently, graphene.

Due to the low surface energy of polymers, gold is commonly combined with titanium or chromium to increase its adhesiveness to the polymer substrates [36]. However, exposure to titanium or chromium in the body can be damaging due to the toxicity of these metals. The use of ITO electrodes in optogenetic implants has been preferred by some works [25, 26] due to its transparency and high conductivity, but its brittleness makes it undesirable in large area flexible implants. Some works have also used conductive polymers as electrodes to increase the charge storage capacity of microelectrodes by improving the charge transfer between the ionic-to-electronic charges [3].
Electrode deposition and patterning of these materials depend on the substrate and the application. For electrode arrays with tracks and contact pads, evaporation or sputter deposition is commonly performed. Evaporation involves generating a vapour from the source material, which is then transported to the substrate and condensed to form a thin film on the substrate. This is a physical vapour deposition method. Other methods that are mainly chemical, involve gas and liquid-based chemical processes. Methods like reactive sputtering and glow discharges combine both physical and chemical deposition [39].

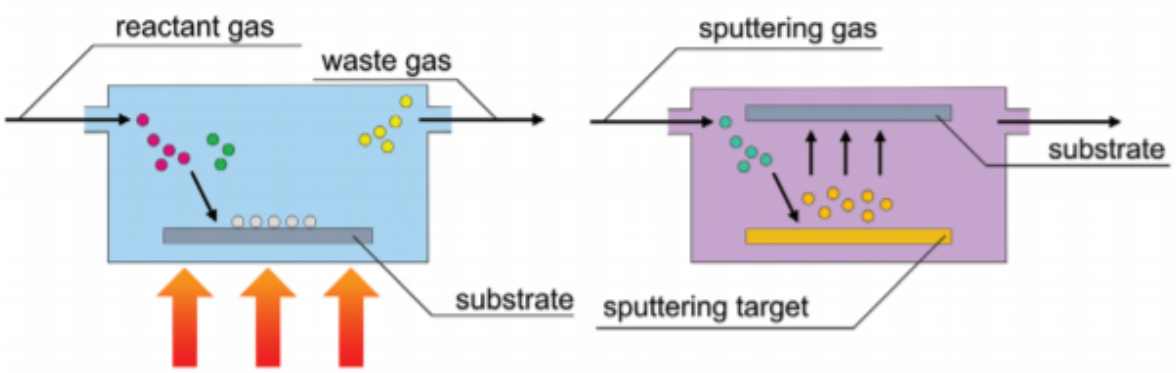

Figure 2.3: Thin Film Deposition and Sputtering shown side by side [32]

The deposited metal can then be patterned using photolithography, microcasting or laser patterning. Microcasting involves heating solid metal into liquid and loading it into channel moulds such as PDMS to develop features with micron-scale precision [6]. Both photolithography and microcasting involve the use of masks or moulds to expose the area to be patterned. Laser-patterning, however, is directly exposing the deposited metal to a high energy laser which is faster because there is no need to wait for the fabrication of a metal mask. Laser-patterning can allow for roughened electrode surfaces, which have been shown to increase the surface area while also promoting cell adhesion to the surface, and improving electrode stability and performance[12].

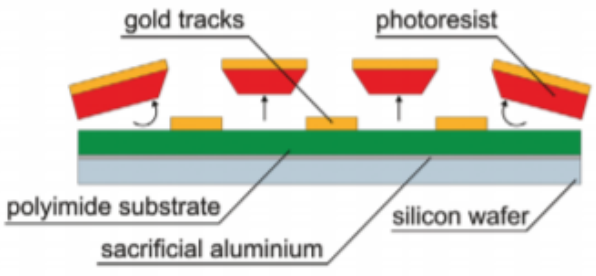

Figure 2.4: Photolithography [32]

These patterned electrode arrays are mostly implemented on flexible substrates in single layers due to the higher chance of failure and the complicated fabrication procedures in multiple layers [11]. By using only a single layer, the number of electrodes on the array is limited due to the lack of space available for the interconnects. However, multiple metal layers allow for denser electrode arrays that increase the overall spatial resolution of the device. The density is limited by the size and inter-electrode spacing of the electrodes. One

such high spatial recording device was implemented by Viventi et al. [47], where flexible silicon electronics technology was used to design a 360 channel electrode array (300x300μm electrode) on a PI substrate. This high density was achieved by introducing two layers of Cr/Au between PI as insulation material which allowed for a large number of interconnects to the electrodes. Even though it was used to measure sleep spindles in cats acutely, no information about the chronic behaviour of the device was provided[47].

2.4. Thin Film Technology in Optogenetics

Thin film technology (TFT) is used to implement layers in devices that are few nanometres to few tens of micrometres in height. From the substrate to the metal layers, the height is limited to these few micrometers. In some cases, encapsulation is used to protect the device from external agents to increase the lifetime of the device, the thickness of the encapsulation is, however, dependent on the application of the device. Thin film substrates such as PI, parylene-C or Polyethylene Napthalate (PEN) have been used to fabricate thin-film ECoG arrays with thicknesses of the array ranging from ~ 6 [22] to 30 μm [34]. The main contribution to the thickness comes from the substrates employed rather than the metal layers, which contribute around 70 to 200 nm to the total array thickness. A thin film electrode array by Hara et al. [13] uses parylene-c and platinum, as substrate and electrode material respectively, to fabricate a 12 μm thick sheath array. The sheath is provided for ease of placement with microwires during implantation. Parylene was used both as a substrate and as an insulation layer to maintain the flexible structure of the array while the platinum contacts between them were exposed using O_2 reactive ion etch [13].
In optogenetics, most arrays designed for simultaneous stimulation and recording range around 65 to 75 m in overall thickness [21, 26]. An increase in the overall thickness of the device could result in loss of flexibility, so care must be taken to ensure that the implant thickness is limited. Also, most of the optogenetic ECoG arrays mentioned here are used for applications that cover small areas when implanted in mice or rats. With dimensions of ~2.5 x 2.5 mm to ~4 x 3 mm, these arrays cover specific regions on the surface of the cortex such as the visual, motor or somatosensory cortex of the brain [21, 26]. By opting to cover smaller areas, information from adjacent neural groups are lost.
The use of TFT, which has commonly been used for large-area active matrix OLED displays, allows the fabrication of large-area optogenetic arrays so that the entire cortex of a mouse can be simultaneously stimulated and recorded with no delay. Smith et al. [40] used an active matrix transistor array on PEN foil to drive OLEDs for optical stimulation and inhibition of neurons. By opting for OLEDs driven by thin film transistors it was possible to control individual pixels on the OLED display to stimulate specific neural tissue. This also reduced the amount of heat generated at the OLED-tissue interface as only a single or few OLEDs are required to be turned on to excite or inhibit local regions of neural tissue [40]. Although no recording points were included in the array, the overall thickness was a little over 125 m which reduces the conformability of the array. In place of PEN, Kim et al. [23] used a parylene-c substrate to fabricate a 2 μm thin OLED device using sputtered thin films of aluminium and ITO, as cathode and anode respectively. The resulting device has a significantly large light emission area of 4 mm^2 for each OLED, reducing the specificity mentioned by the previous work .

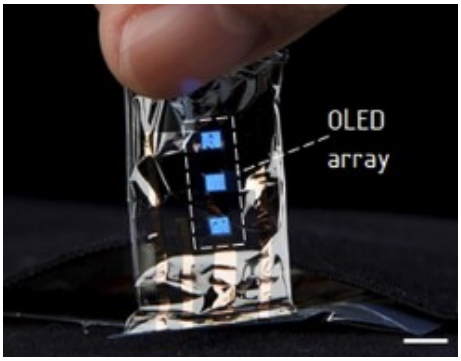

Figure 2.5: OLED array on a parylene-c substrate of 2 μm thickness [23]

2.5. Chapter Conclusion

In this chapter, we discuss the substrates commonly used for flexible neuromodulation arrays and identify suitable characteristics of a flexible substrate for optogenetics onto which μLED integration is possible. The integration techniques for these μLEDs are shown to vary from growing GaN-based μLEDs on a sapphire substrate to integrating commercial μLEDs using a PDMS stamp for alignment. We also discuss favourable electrode materials, (Au, ITO, Pt) and their deposition and patterning techniques that allow for multiple metal layers to increase the available electrode density. In the end, we discuss the use of thin film technology to implement optical stimulation and recording on a single large-area array.

Previous works discussed that utilize thin-film technology using flexible substrates either have only electrodes for recording[13, 22], only allow stimulation using OLEDs [23, 40] or do not have large number of electrodes and light sources to cover the entire cortex [49]. Our goal is to integrate commercial μLEDs onto a large-area high-density ECoG array fabricated using thin-film technology. The μLEDs will be integrated using a pick and place tool. This array should be large enough to cover the cortex of a mouse's brain, and have individually addressable stimulation and recording points around the Primary Motor Cortex, Primary Visual Cortex and Primary Somatosensory Cortex.

3

Methods

3.1. Design of Flexible Large Area Optogenetic Array

The design of an optogenetic array that covers the cortex of a mouse's brain was initially focused on simple considerations, such as:

- The size of the array
- Number of stimulating and recording units that can be accommodated in the given space
- The pitch between stimulating and recording units
- The diameter of the electrodes
- • Physical arrangement of the optical stimulation sites on the array

However, before the array is designed, the ideal materials for the substrate, the electrodes and the LEDs need to be chosen for this particular array. Based on the substrate materials discussed in Chapter 2, PDMS stands out as a result of its Young's Modulus being much closer to that of the brain. Even so, handling this material proves to be difficult during implantation which encourages for another material choice. The 2.5 GPa Young's Modulus of Polyimide (PI) although much higher than PDMS (~100 kPa) makes the implant easier to handle during tests and implantation. PI is also more preferable in this design because of the similarities that exist in processing PI to that of common microelectronics. Since PI is also used as a substrate extensively in the TFT processing for flexible displays at Holst Centre, it is chosen for this array as there is a lot of experience in processing this material.
Gold (Au) was chosen as an electrode material due to its high conductivity and chemical stability. However, due to its poor adhesion with polymers, a 78 nm thickness layer of Au/Ti was sputtered to increase its adherence with the PI film.
For the optical stimulation, commercially available μLEDs (CREE TR2227TM) with 220×270 μm dimensions, and peak wavelength at 460 nm were used. These μLEDs provide blue light for activation of Chanelrhodopsin-2 and were integrated into the array with a pick-and-place machine, followed by Isotropic Conductive Adhesives (ICA) bonding.
The proposed final device is shown in Figure 3.1, and includes a ZIF (zero insertion force) connector bonded to one end of the array to facilitate μLED driving and recording signals from the electrodes.

3.1.1. Shape and space considerations of Optogenetic Array in Mouse Cortex

An array covering an area of 6 mmX5 mm was adopted in this design to comply with specifications given by neuroscientists at Erasmus MC. The primary points of interest are indicated in Figure 3.2 by red dots, with M1, S1 and V1 representing, primary motor cortex, somatosensory cortex and visual cortex respectively. The blue points on the image indicate alternative positions for μLED placement in the case that would not be possible to accommodate the μLEDs in the red points.
It is possible to execute a simple design with just 6 μLEDs to stimulate only the required points. However, in doing so, there is a possibility of losing reactions and responses from adjacent areas that might occur from the

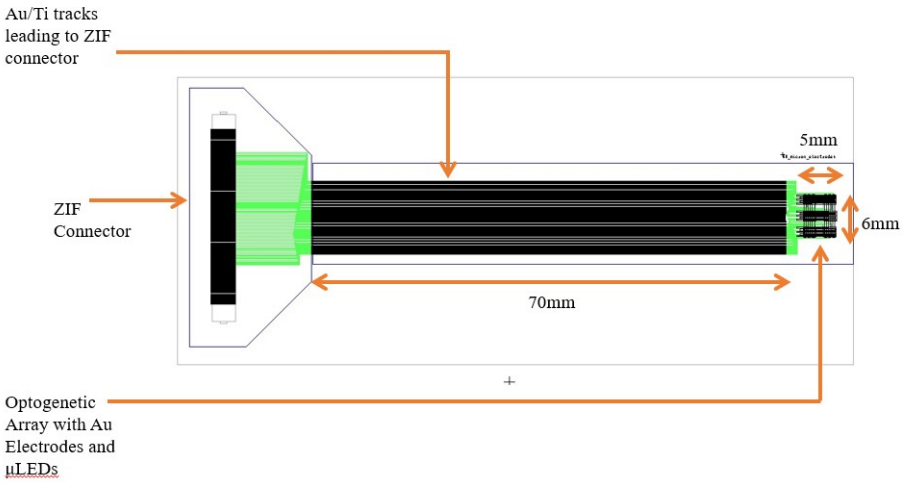

Figure 3.1: Proposed device design with ZIF flex connector

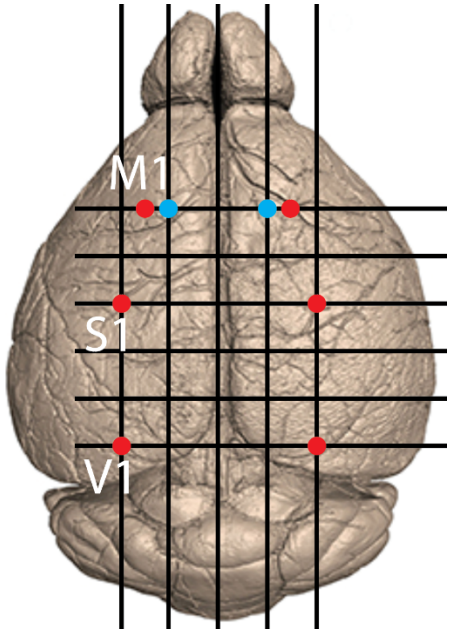

Figure 3.2: A mouse brain with reference points for Primary Motor Cortex (M1), Somatosensory Cortex (S1) and Visual Cortex (V1)

optical stimulation around the stimulated area. The use of just 6 stimulation sites would also call for larger μLEDs to stimulate efficiently a large area, thus reducing the flexibility of the device. By opting to use more stimulation sites, it is possible to incorporate smaller μLEDs while maintaining the mechanical flexibility of the device. Furthermore, other locations along the cortex can be stimulated in case additional studies of neural pathways elsewhere are required. By incorporating more than just few stimulation and recording sites on the array, the resolution of the device is significantly increased.

Following the design choice to incorporate more μLEDs, the next consideration is the shape of the array, where a choice between a rectangular and a circular array was made. Based on dimensions of 6 mm × 5 mm, the area covered by the rectangular array is 30 mm^2 (length × breadth) while the area covered by the circular array is 33.165 mm^2 (π × radius^2). Although the circular array covers a larger surface area, it can be observed in Figure 3.3 that the required points of interest, specifically the V1, is not covered sufficiently with enough electrodes around it. This could result in loss of information after a successful stimulation.

To sufficiently encompass all the points of interest on the cortex to ensure uniform stimulation, a rectangular array was chosen.

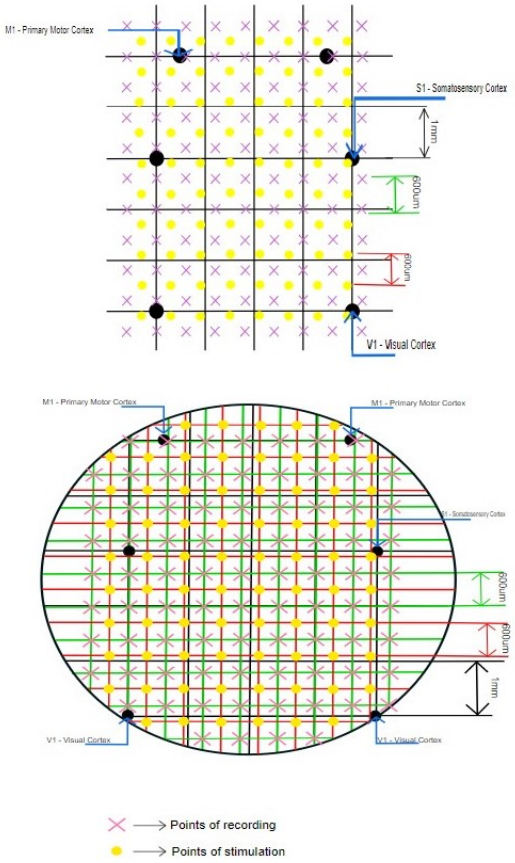

Figure 3.3: Initial designs of array with rectangular and circular shapes

3.1.2. Arrangement of recording and stimulation sites on the Array

The arrangement of electrodes and μLEDs on the optogenetic array is a key factor in the performance. This is because too much space between the μLEDs reduces the intensity required to activate the ChR2, resulting in no occurrence of stimulation. Similarly, too much space between the electrodes results in loss of information from adjacent neuronal groups. Alternatively, if the pitch between the μLEDs is less, the heat generated from the μLEDs will not be allowed to adequately dissipate leading to increased chances of tissue damage at the implantation site. A reduced pitch between electrodes could result in crosstalk and introduce noise in the recorded signal. It is also important to lay out the electrodes and μLEDs such that simultaneous stimulation and recording is possible in a particular location without loss in the temporal resolution of the array.
To develop such an arrangement, the primary design involved a pitch of 1 mm between each electrode and between each LED, with a pitch of 500 μm between an electrode and a LED. However, the μLEDs employed in this design have dimensions of 270 μm × 220 μm with a minimum driving voltage of 2.7 V. These dimensions allow stimulation up to 1.2 mm in the horizontal distance [26]. As the optical intensity decreases with distance, the μLEDs were placed with a pitch of 600 μm to ensure uniform stimulation without the need for a higher driving voltage. The space between the electrodes were also reduced from 1mm to 600 μm such that the area under stimulation by the μLEDs were sufficiently covered by the electrodes to increase the resolution of the recorded signals, with a pitch of 300 μm between an electrode and a μLED.

3.1.3. Routing Considerations for I/O lines on the Array

Following the design of the array given in Figure 3.4, the next step was to connect leads from the electrodes and the μLEDs to the bonding pads. The initial design envisioned all the electrodes and the μLEDs on a single layer of PI substrate connected to a ZIF connector which would lead to outside the mouse's brain. Interconnects from electrodes and μLEDs of 60 μm thickness were used to route all the connections to the ZIF connector. To avoid cracking of these interconnects during handling, the goal was to route most of the connections through the middle of the implant. This proved difficult because of the lack of space on the

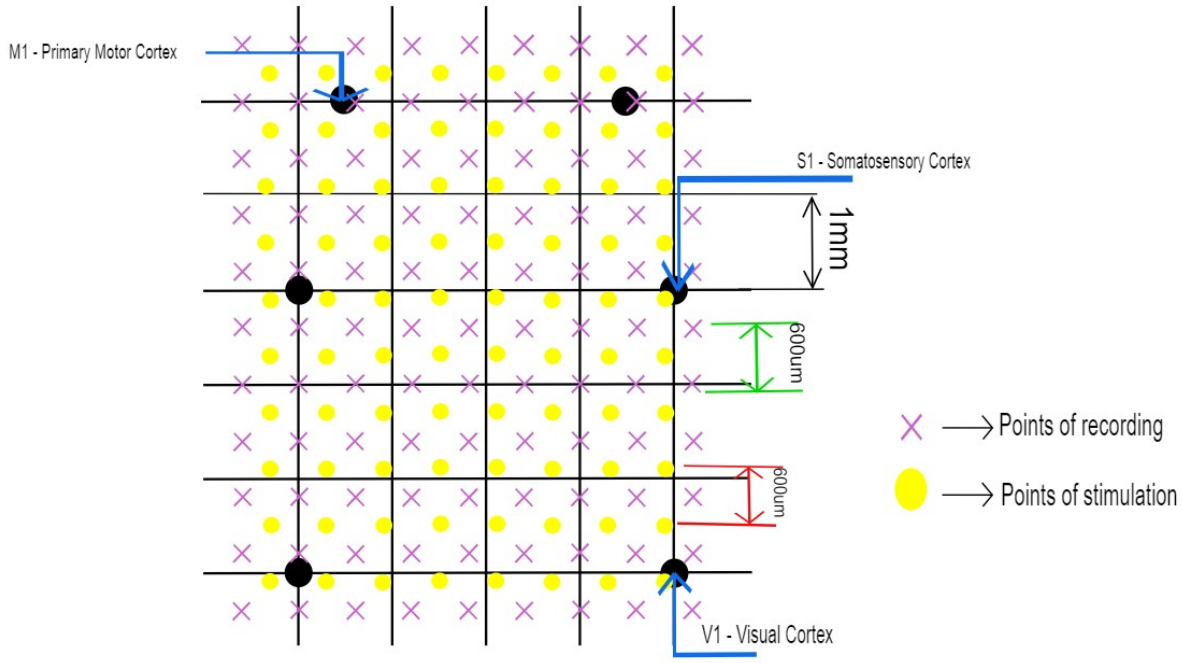

Figure 3.4: Rectangular optogenetic array with electrodes and μLEDs separated by a pitch of 300μm

monolayer array. A number of electrodes and μLEDs were removed to make room for the interconnects, but this was done by ensuring that the points of interest were still sufficiently covered by electrodes and μLEDs all around them (Figure 3.5).

Still, routing proved to be challenging because of the presence of clustered electrodes and μLEDs around

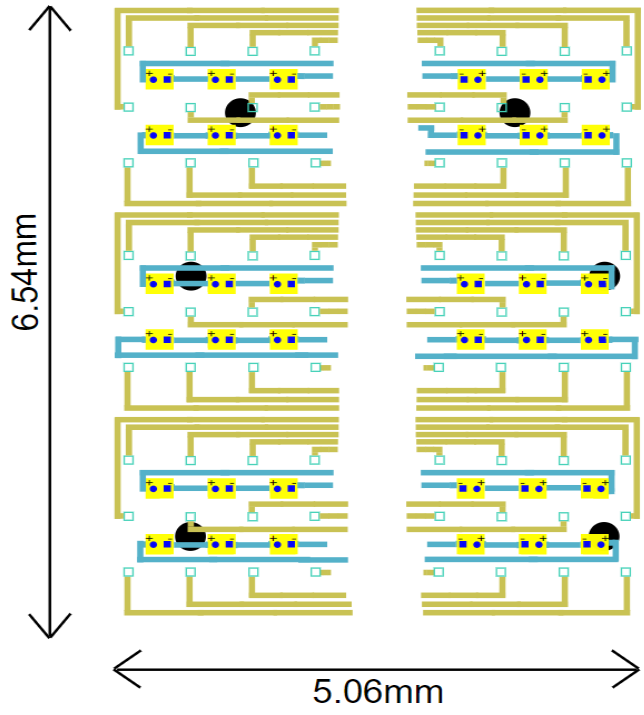

Figure 3.5: Rectangular optogenetic array with fewer electrodes and μLEDs for routing

each point of interest. Even reducing the thickness of the interconnects proved to be of little use.
A monolayer approach to the optogenetic array was thus reconsidered and resulted in the design of two layers of Au/Ti interconnects with a Silicon Nitride (SiN) dielectric layer between them. This allowed for more space to route the interconnects in each metal layer. The horizontal interconnects supplied the bottom metal layer while the electrodes and the vertical interconnects supplied the top metal layer. Vias introduced in the SiN layer provided contact between the two metal layers and also openings for the electrode to make contact with the mouse brain. A schematic of this design is provided in Figure 3.6 and Figure 3.7.

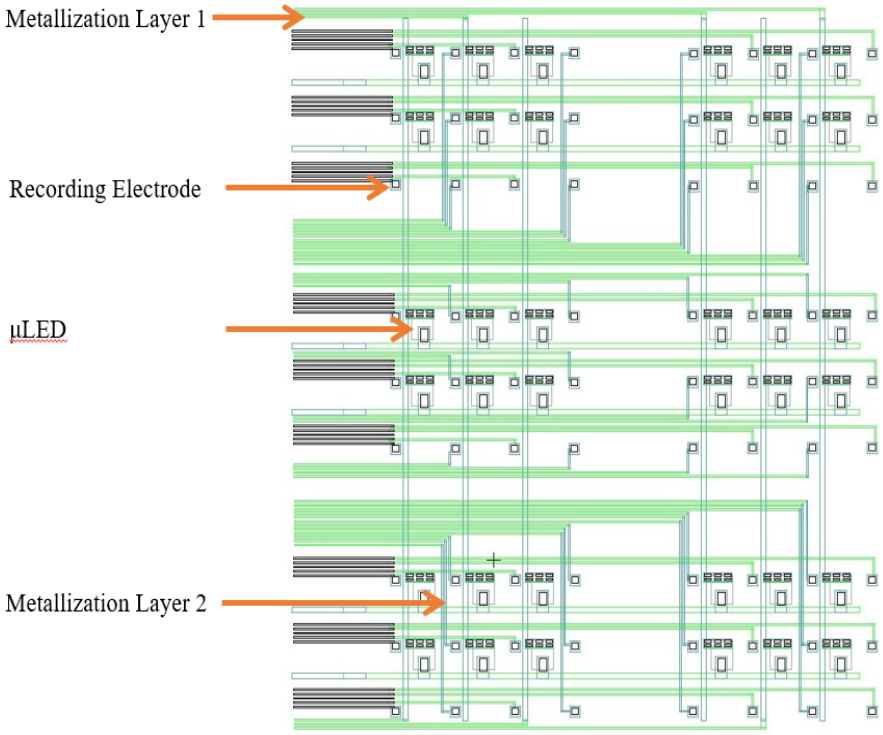

Figure 3.6: Optogenetic array with two metallization layers separated by a dielectric

3.2. Fabrication of Flexible Large Area Optogenetic Array

Thin film technology is generally used when bulk materials cannot be reduced to the required dimensions for a particular application. It involves physical and chemical vapour deposition methods to deposit films of sub-micron thicknesses very fast or alter the surface chemistry of particular films on the substrate. For this optogenetic array, four layers of thin films were deposited and altered, based on the required design shown in Figure 3.7.
On each 6 inch glass substrate, four samples were placed to optimise available resources and minimise the number of plates subjected to each phase of lithography (Figure 3.8).
The Au/Ti sputtering was performed at Philips Innovation Labs (PInS) while the rest of the lithography steps

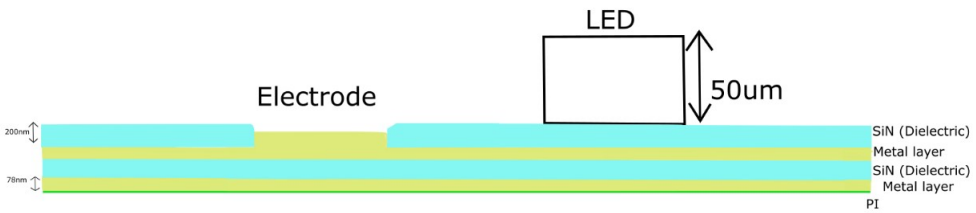

Figure 3.7: Topography of the flexible optogenetic array with various layers of thin films

were carried out at the Holst Centre cleanrooms.

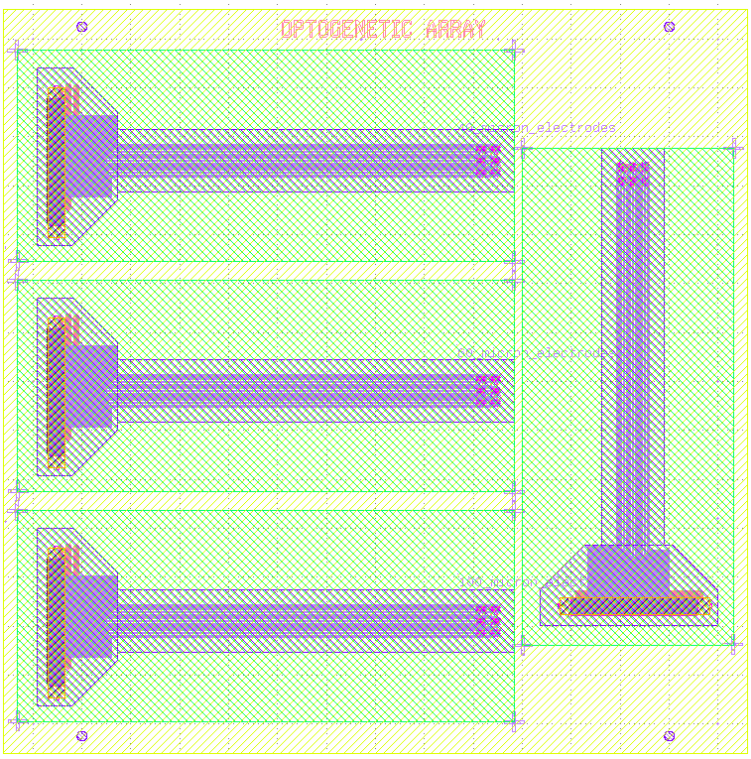

Figure 3.8: Design of the 6 inch glass wafer with 4 optogenetic arrays

3.2.1. Au/Ti Sputtering and Etching

The first metal layer (Au/Ti) was sputtered on a glass with PI of 14 μm thickness. This was a uniform 78 nm layer with 3 nm of Ti, followed by 75 nm of Au. After deposition of the Au/Ti layer, lithography steps were employed to define the first set of interconnects on the substrate.

The samples were spin coated with a negative photoresist followed by a laser scanning lithography using Direct Write Laser Lithography System by Heidelberg Instruments for the pattern definition. This is a maskless lithography process that exposes the photoresist to a focused electron beam so as it can be developed later. Since a negative photoresist was used, during development, the area on the PI not exposed to the laser is removed using an AZ developer. To harden the resist, the samples are placed on a hotplate heated to a 120 °C for 2 minutes.

The etchant for gold was prepared by mixing 50 ml of an iodine-iodine TFA gold etchant with 150 ml DI water. The sample is soaked in this etchant and a visual inspection on the surface of the sample was performed to ensure that the wet etching was successfully done. This is followed by thoroughly rinsing the sample in DI water and placing the samples in Avenger Ultra-Pure 8 Spin Rinse Dryer to rinse the substrates without leaving any water spots. The titanium was then etched away by soaking the samples in a titanium etchant, TFTN, heated to 60 °C for 7 minutes. The sample was then once again rinsed in DI and placed in the Spin Rinse Dryer.

The process flow as discussed is shown in Figure 3.8. The etching of the first layer of Au/Ti is completed by stripping the photoresist which was followed by rinsing and drying the samples.

3.2.2. SiN Deposition and Introduction of Vias

A PECVD deposition system, Elettrorava, was used to deposit 200 nm of SiN at 250 °C on the patterned Au/Ti layer on the samples. The samples were rinsed and dried, and then a layer of oxygen plasma was applied by a RIE etcher to remove any particles introduced during SiN deposition.

To pattern the vias on the SiN, photoresist had to be spin coated first. However, SiN has poor adhesion to photoresists, therefore, a HMDS primer was applied onto the SiN layer by placing the samples in a low pressure oven heated to 120 °C for 25 minutes. The samples were then cooled, allowing the photoresist to be applied.

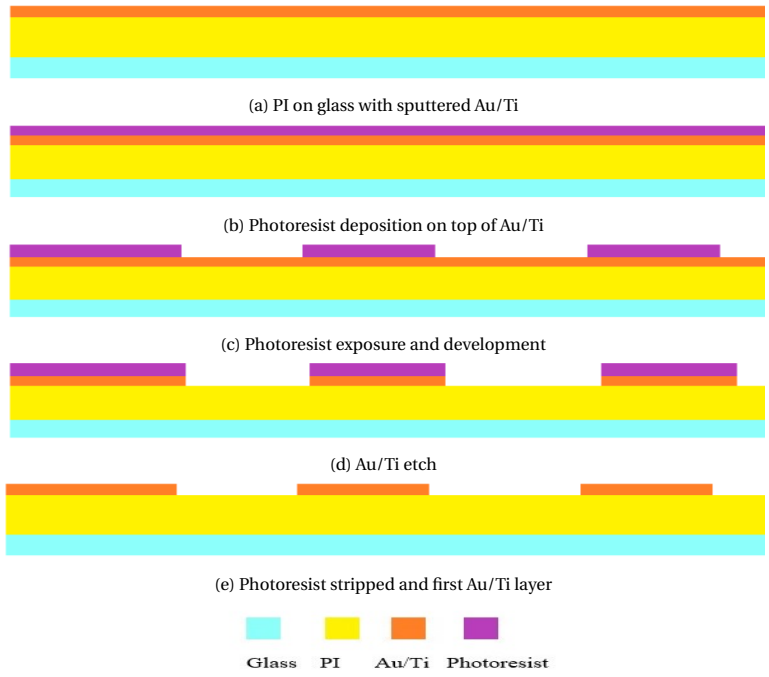

Figure 3.8: Processing steps for the fabrication of the first Au/Ti layer

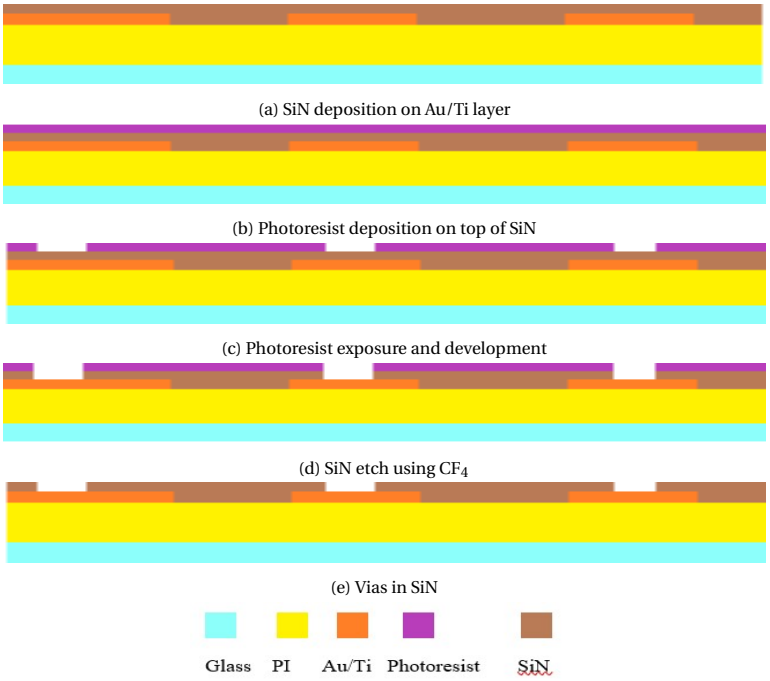

Figure 3.9: Processing steps for the fabrication of vias on the SiN

Samples coated with the negative photoresist were placed on a hotplate (95 °C) for 2 minutes to harden the resist.
The samples were once again exposed using the laser lithography tool to pattern the vias on the SiN, and then developed using the AZ developer. A dry etch by CF_4 was used to open the vias on the SiN in a downstream plasma RIE etcher where the samples were set down for 260 seconds. The photoresist was then stripped and the samples were rinsed in DI and dried in the Spin Rinse Dryer.

The steps mentioned in sections 3.2.1 Au/Ti Sputtering and Etching and 3.2.2 SiN Deposition and Intro-

duction of Vias are repeated to create the remaining two layers shown in Figure 3.7, after which the samples are cut and separated from each on the glass substrate.

3.2.3. System Integration

The electrode array was sent to PInS Greenhouse to bond the μLEDs and the ZIF connector using Istropic Conductive Adhesives (ICA). A pick and place tool was used to individually bond each μLED to the array.

3.3. Characterisation Methods

Succeeding fabrication of the optogenetic array, characterisation of the implant was performed to determine whether Thin Film Technology can be used to implement a flexible large area optogenetic array device that can withstand the evaluation methods discussed in the following sections.

3.3.1. Electrochemical Impedance Spectroscopy

Evaluation of the performance of the Au/Ti electrodes on the array was required to observe its behaviour in specific scenarios. The effect of saline (Phosphate Buffered Saline) on the electrodes were characterized to measure the variations in the impedance values of the array over a range of frequencies. The electrochemical impedance spectroscopy (EIS) is used to understand the behaviour of the electrode-electrolyte interaction based on the reactions that occur on the electrode surface. The reactions can be oxidative or reductive, if irreversible reactions occur which alter the surface of the electrodes, or reversible reactions occur, where there is purely charge transfer between the electrode and the electrolyte interface. These reactions occur when a small AC voltage is applied to overcome the double layer capacitive charge around the electrode in the saline solution while the frequency is varied between 0.1 Hz to 1 kHz. The behaviour of the electrode over different values of frequency overtime was studied.
The measurement system is composed of a working electrode, a reference electrode and a return electrode. The working electrode here is the Au/Ti electrode, while Silver/Silver Chloride is the commonly used reference electrode and the return electrode was selected such that it had a low impedance and did not affect the impedance values of the working electrode during measurement.

3.3.2. Characterisation in Phosphate Buffered Saline

Soaking the array in PBS during EIS allowed the observation of the performance of the electrodes in a wet environment. Determining the performance of the entire optogenetic array in a wet environment is, however, crucial to estimating the longevity of the implant in in-vivo conditions. The use of PBS allowed the samples to encounter reactions similar to that of the body as ionic concentration of components in PBS was very similar to that of the extra cellular fluid (ECF) in the body, as shown in Figure 14. For this reason, a 1 × PBS solution was prepared with 1L of water to obtain a PBS solution with 0.0027 M KCl and 0.0137 M NaCl, and a pH of 7.4. Samples were soaked for 1 week each in 37 °C to mimic body temperature and then observed under a profilometer to note the change in the topography of the SiN on exposure to PBS following the soak. Samples were rinsed with DI and dried before and after soaking in the PBS.

	ECF / mM	0.01M PBS / mM
Na^+	147	153
Cl^-	113	140
K^+	2.90	4.20
PO_4^{3-}	0.358	9.57
Ca^{2+}	1.14	—
Mg^{2+}	1.10	—
HCO_3^-	23.3	—
pH	7.3	7.4
Conductivity		
25 °C	1.45 S/m	1.60 S/m
37 °C	1.79 S/m	2.00 S/m

Figure 3.10: Ionic Composition of ECF and PBS [4]

3.3.3. Thermal Characterisation

Among the challenges faced in designing a wireless optogenetic array is the localised heating of the tissue beneath the μLEDs. This heating effect was also minimised by operating the LEDs at a low driving voltage, just enough to elicit a response from the neurons. The alteration of the duty cycle of the LEDs was also used to determine its effect on the time required for heat dissipation of the μLEDs. An Arduino Mega 2560 was used to control the μLEDs on the array by varying their duty cycles using PWM method. LEDs with duty cycles of 10%, 30%, 50%, 70% and 90% were investigated with an overall time period of 100 microseconds during which the μLED was switched ON and OFF. By using a thermal infrared (IR) imager, the thermal variation of a single μLED was investigated under different voltages and different duty cycles.

4

Results and Discussion

4.1. Microfabrication

The layers of the array as given in Figure 3.7 were fabricated sequentially on the Polyimide (PI) substrate. Due to the relatively new aspect of the design for the optogenetic array using thin film technology, the samples were inspected after every deposition, exposure, patterning and etching to ensure the standard of the sample was maintained throughout the fabrication. In this section, the hurdles faced during the fabrication process and the steps taken to overcome them (described in Section 3.2) are documented and discussed.

4.1.1. Au/Ti Layers

Following the process flow discussed in Section 3.2.1, a layer of Au/Ti was sputtered on the glass wafer and subsequently etched. Later, a visual inspection was performed under an optical microscope. Since gold is etched by manually soaking the sample in the etchant and gently washing the etchant over the sample while waiting for the gold to be etched from the PI , occurances of overetching were observed on some interconnects leading to the array. The images shown in Figure 4.1 are examples of such overetching, which if too large can increase the resistance of the interconnects due to decrease in overall area of the thin film Au. In this design, the feature sizes (~ 15μm) of these thin film interconnects are large enough that even under a scenario of overetching, the total resistance of the interconnect is not significantly affected.

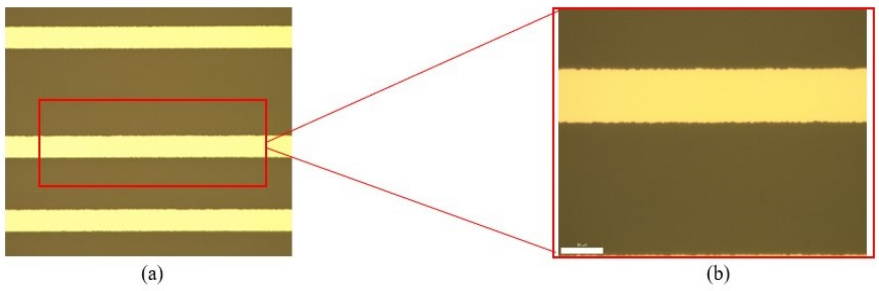

Figure 4.1: Au interconnects showing overetching In (a), three interconnects of 15 μm width with signs of overetching on the edges is shown. In (b), a maginified image of one of the interconnects with clear overetching on the edges

4.1.2. SiN Deposition and Vias

Following the patterning and etching of the Au/Ti layer, 200 nm of SiN was deposited using a PECVD tool, Elettrorava. Then, the SiN layer was patterned and etched to introduce vias as described in section 3.2.2 SiN Deposition and Introduction of Vias. During this step, an old recipe was chosen with 900 W of power, for 260 seconds, using CF_4. This resulted in vias larger than 10 μm and bite-shaped edges at the juncture where the vias open past the gold interconnects as can be observed in Figure 4.3. The larger vias did not impact the quality of the contacts because the second metallization also used a 78 nm layer of Au/Ti. For the final SiN layer, the power for the dry etching was reduced to 100 W for 130 seconds. Since the final SiN layer opens

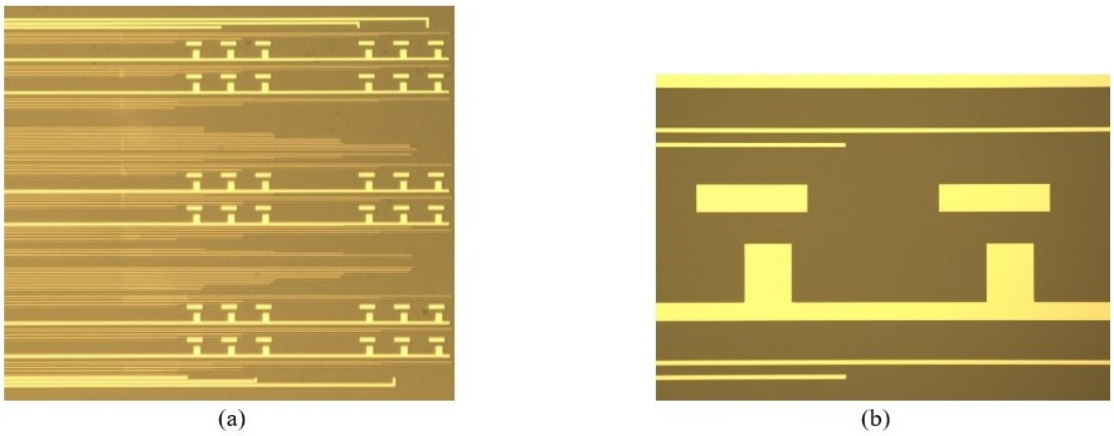

Figure 4.2: First Layer of Au/Ti on PI. In (a), the entire array is shown. In (b), a magnified image of the array with the anode and cathode connections for the LED is shown.

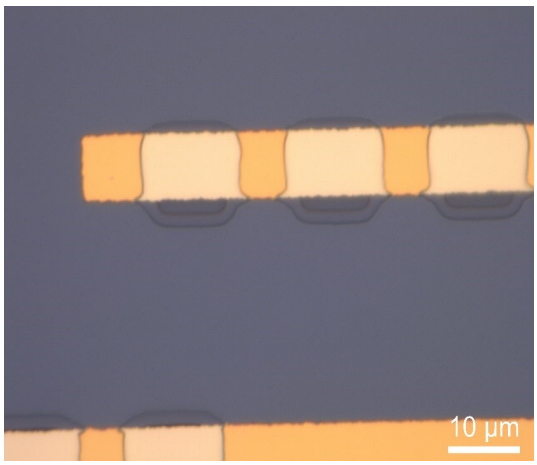

Figure 4.3: Au/Ti interconnect showing vias on SiN larger than conceived with bite-shaped edges at the junction of Au/Ti

contacts for the electrodes, and vias larger than what was required will also expose the interconnects to the cortex of the mouse during stimulation and recording. This would affect the recordings of the electrode array and alter the collected data, but the reduction in power from 900 W to 100 W proved essential in obtaining evenly etched electrodes and, anodes and cathodes.

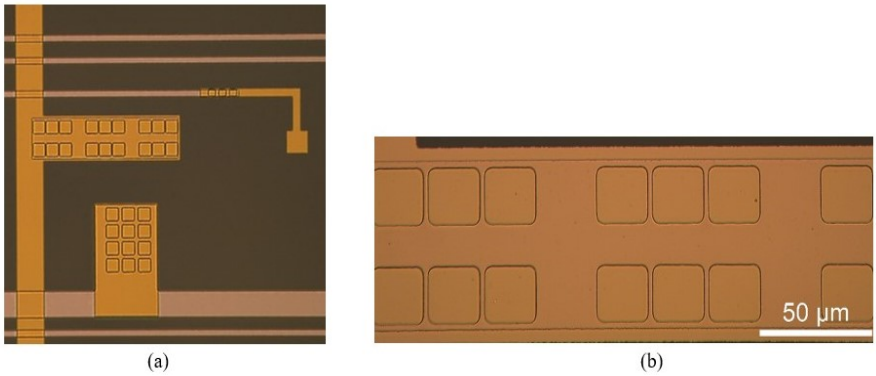

Figure 4.4: Magnified image showing (a) anode and cathode connection for the LED with vias and an electrode on the right and (b) anode with patterned vias after final layer of SiN deposition and patterning

4.1.3. Lasering of Glass and PI

Once the final layer of SiN was opened for vias formation, the unconsumed PI layer around the array was removed using a laser and four samples separated from the 6 glass plate. An inaccuracy during the lasering affected the interconnects which resulted in the loss of 6 samples.

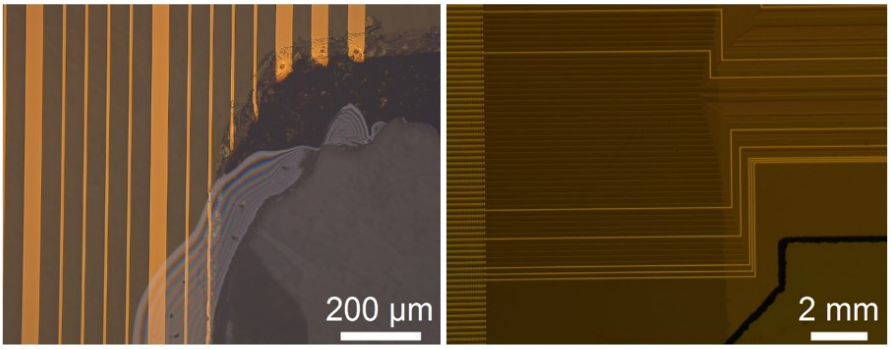

Figure 4.5: Post lasering of the PI in which (a) shows interconnects being damaged due to error in design and (b) shows a good lasered PI substrate on glass

4.2. Wet Characterisation

Following the microfabrication, the samples were soaked in PBS solution so as to predict the performance of the array in an environment similar to the brain. This was accomplished using two different protocols: the first, used PBS, pH 7, at room temperature for 1 week to evaluate the performance of the electrodes; the second, used PBS, pH7, at 37°C to estimate the degradation rate of the passivation layer. The performance of the passivation layer on the samples was inspected using a profilometer before and after a period of 1 week at 37°C.

4.2.1. Electrochemical Impedance Spectroscopy

The electrochemical impedance spectroscopy (EIS) is a technique used to investigate properties of materials and electrode reactions. The electrochemical impedance is measured by applying a small-signal AC potential to the electrochemical cell using a reference electrode of Ag/AgCl and the resultant current being measured by a counter electrode made of Platinum. The Ag/AgCl electrode is used because of its half-cell potential that does not change with time or change in temperature. It ensures the stability of the EIS setup. The counter-electrode which is generally much larger than the working electrode is used to reduce the overall impedance. The electrodes were characterized to investigate and evaluate their impedances at different frequencies over

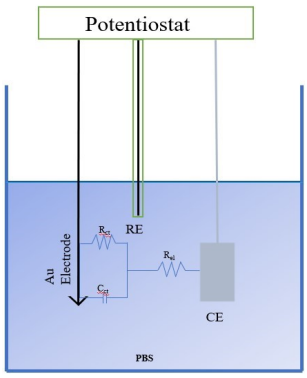

Figure 4.6: Schematic for EIS measurement indicating equivalent circuit models

time. The response of the electrodes in PBS at room temperature over a course of 1 week were studied using the Biologic Potentiostat. Initial impedance of the electrodes at 1 kHz range at 6.28 kΩ which increases up to 7.48 kΩ on day 3 and reduced to 7.04 kΩ by the end of day 6 (Figure 4.7b). This increase in impedance

in the initial days followed by subsequent marginal decrease is also observed at lower frequencies, namely 0.1 Hz, 10 Hz and 100 Hz. However, the increase in impedance from day 0 to 3 is significantly larger at lower frequencies. This increase in impedance in the initial days is similar to other works which explore stability of gold electrodes over time [15, 16].

This initial increase of impedance can be linked to adsorption of phosphate ions on the surface of the gold electrodes which decrease the available surface area on the electrodes. Since at higher frequencies the main contribution to the electrochemical impedance is that coming from the electrolyte (R_{el})(in Figure 4.6), the change in impedance observed in this frequency is much lower. At lower frequencies, the effect of reduced electrode area after the initial measurement is more prominent because of the significant contribution of the R_{ct} (in Figure 4.6) to the impedance. In the following days the measured impedance remains stable over time, showing little to no change at the different frequencies, indicating stable performance of the Au/Ti electrodes over time.

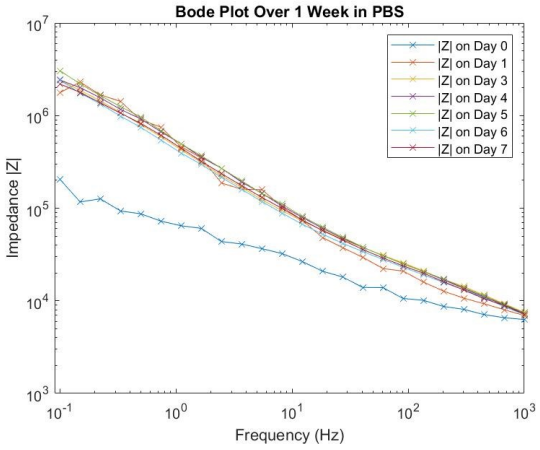

(a) Bode Plot of Au/Ti electrode over a period of 1 week

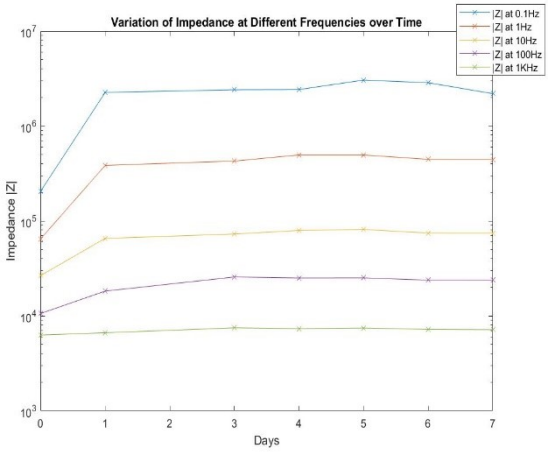

(b) Impedance at 0.1 Hz, 1 Hz, 10 Hz, 100 Hz and 1 kHz over 1 week in PBS

Figure 4.7: Results for EIS of Au electrodes

4.2.2. Characterisation of Passivation Layer

All the samples have a layer of SiN above the final Au/Ti layer with vias opened on the SiN above the electrodes. SiN was deposited to separate and insulate the Au/Ti tracks from direct exposure to the surroundings of the implant when placed on the mouse's cortex. If the Au/Ti tracks were to be exposed to the ionic environment of the brain, the interconnects would also conduct signals along with the electrodes leading to poor resolution of the array. Since these interconnects also have a smaller surface area and longer length compared to the electrodes, the overall resistance of the array increases upon exposure to the environment in the brain. Since the performance of SiN in-vivo affects the quality of the recorded signals overtime, a setup was put

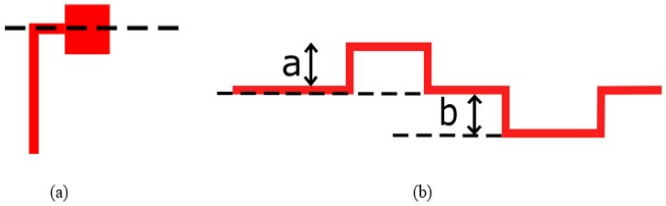

Figure 4.8: (a) Top view of the area considered under the profilometer and (b) Front view of the profile under consideration

together to study the behaviour of SiN on the samples at 37°C in PBS as discussed in Chapter 3. However, before soaking the samples, the profile of the sample was observed and measured under a profilometer. The profile used to observe the SiN behaviour is given in Figure 4.8. The front view of the profile indicates height of two regions specifically, with a depicting the height of the SiN above the interconnect to the electrode while

b shows the depth of the via leading to the Au/Ti electrode.
The change in the profile around this area was once again measured after removing the samples from PBS and rinsing them with DI water. The before and after height of a and b for three rows of electrodes on the array are given in Table 4.1.
The decrease in the height of the SiN layer is observed in all the three rows observed indicating a possible

Before (in nm) (a)	**After (in nm)** (a)	**Before (in nm)** (b)	**After (in nm)** (b)
80	68	23	23
75	70	29	28
78	73	32	25

Table 4.1: Change in height of SiN before and after 1 week soak in PBS measured using profilometer

dissolution of SiN in PBS. Although this dissolution is not inherently a disadvantage because the implant was designed for acute experimentation over the course of 4 to 8 weeks. SiN is already known to have high dissolution rate [41]. Despite its low ion diffusivity, there is a high likelihood that the metal layer beneath the SiN can be exposed during the end of these soak tests and influence the signals being recorded. This exposure can also attack the thin Au/Ti interconnects leading to broken contacts disrupting the function of the implant.

4.3. μLED Bonding

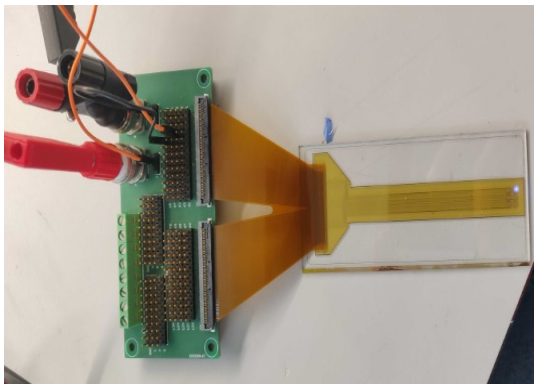

Figure 4.9: Sample Optogenetic Array with a ZIF connector connected to a PCB for LED driving

The μLEDs along with ZIF connectors were bonded to the sample electrode array at the PInS (Philips Innovation Services) Greenhouse facility. To ensure unidirectional conduction of the μLEDs, Isotropic Conducting Adhesive (ICA) was used; for the ZIF connector, Anisotropic Conducting Film (ACF). Upon receiving the initial four samples, a PCB was fabricated and plugged to the ZIF connector of the sample to drive the μLEDs (Figure 4.9). A power supply was varied between 2.7 V to 3.4 V while limiting the current with a 100 Ω resistor in order to limit the current to levels below 20 mA.
During initial assessment, each one of the four samples showed yields lower than 10% for the number of working μLEDs. The calculated yield for 36 μLEDs on each sample is shown in Table 4.2.
The samples were then observed under a microscope to determine the reason behind the low number of

Sample Number	**Yield**
Sample 1	2.7%
Sample 2	0%
Sample 3	2.7%
Sample 4	8.3%

Table 4.2: Sample Optogenetic Array with a ZIF connector connected to a PCB for μLED driving

working μLEDs. A first look at each of the samples showed the μLEDs firmly attached only to the designated cathode and anode on each row and column. There were also some flecks of dried liquid visible on the PI

surrounding the μLEDs. This was present in all the four samples. However, a distinction was observed in Sample 3, where a dried residue seems to connect three μLEDs (Figure 4.10). An initial hypothesis was drawn that the ICA had overflown during bonding, resulting in a short circuit across the columns and rows. This was later disproved because the residue was found to be an underfill material used to strength the connection of the LEDs to the PI which is non-conductive in nature.

A multimeter was then used to check for shorts across each column of the anode and cathode on all the

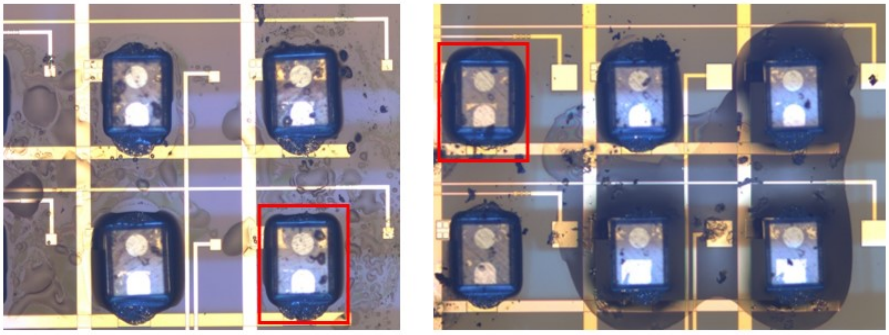

Figure 4.10: Microscope images of Optogenetic Arrays with μLEDs bonded to PI where (a) is Sample 4 and (b) is Sample 3 indicating the function μLEDs in red

four samples. Although no short was found, resistances across the μLEDs were around 2 to 15 MΩ indicating the existence of open contacts across the array. The μLEDs were then checked under an X-Ray and then mechanically separated from the PI substrate to observe the quality of the connection between a working μLED and a defect μLED. The image in Figure 4.11 shows the X-Ray with no difference in the adhesive connection between a working and a defect μLED. The conclusion was then drawn that the problem lied with the ZIF connector bonded to the PI substrate when the connector was easily pulled away from the PI with little force applied. The ACF was not cured properly during bonding leading to poor contact with the interconnects leading to the array. This was the reason behind the high resistances measured with the multimeter.

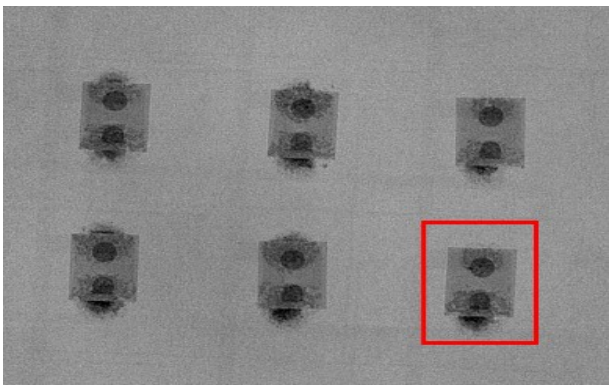

Figure 4.11: μLEDs under X-ray showing good contacts with the underlying array

4.4. Thermal Characterisation

As explained in the previous chapter, the heat generated from the μLEDs during stimulation could damage the tissue around the array. Although during the design considerations for optimal placement of the μLEDs were made to accommodate adequate heat dissipation, the driving voltages of the μLEDs and the duration of stimulation also contribute to the heat generated by the μLEDs. By varying the voltage between 2.7 V and 3.4 V (maximum forward voltage of the μLEDs) at duty cycles of 10, 30, 50, 70 and 90%, the average rise in temperature was measured using a handheld thermal IR scanner.

An Arduino Mega 2560 board was used to send PWM signals to the μLED to vary the duty cycle. The Mega 2560 has a microcontroller on it and 12 pins which provide PWM outputs. Duty cycle is the duration for

which the μLED is ON divided by the total time period of the stimulation. By varying the T_{ON} duration, the duty cycle is varied.

$$Dutycycle = \frac{T_{ON}}{T_{ON} + T_{OFF}} \tag{4.1}$$

The output voltage provided by the Arduino Mega 2560 is a constant 5 V, but the maximum forward voltage of the μLED is only 3.4 V. The μLEDs have to be protected from the 5 V by limiting the voltage with a resistor such that a 20 mA current flows through the μLED at 3.1 V which is typical for the CREETR2227 μLEDs. A 100 Ω resistor was chosen and connected to the μLED so that at 100% duty cycle the forward current through the μLED was 20 mA.
After connecting the array with the PCB to the Arduino Mega 2560, there was the challenge to vary the voltage supplied (2.7 V to 3.4 V) from the Arduino board to the μLED. A potentiometer was connected from the Analog pin (A0) of Arduino Mega 2650 to the the μLED to vary the supplied voltage. Also a code was written such that any change in the position of the knob of the potentiometer read by the analogRead would display the voltage on the Serial Monitor of the Arduino software. As the analogRead values range from 0 to 1023, with 0 indicating 0 V and 1023 indicating 5 V, the output from A0 was divided by 1023 and multiplied by the reference voltage (5 V) to display the voltage at any given position of the potentiometer knob.
The values from the potentiometer were then fed to the PWM pin connected to the μLED by the analogWrite function which writes an analog value from the potentiometer to the PWM pin. The code for varying duty cycle and the voltage is given in the Appendix.

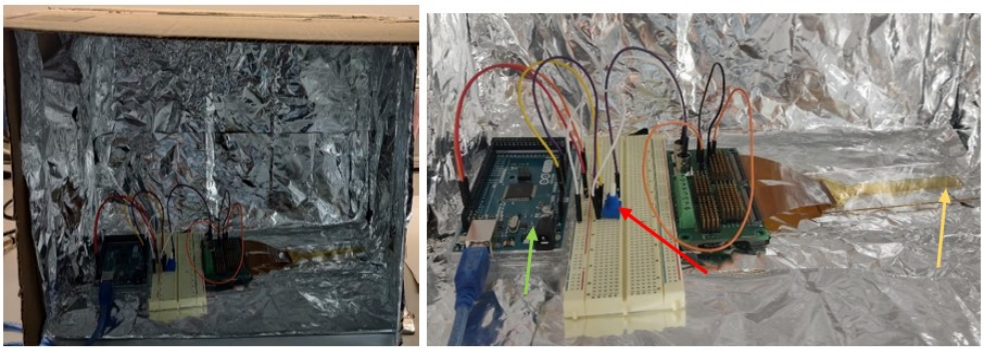

(a) (b)

Figure 4.12: Experimental Setup for Thermal Characterisation is shown in (a) where the Box Lined with Aluminium Foil holds the Arduino, Breadboard and the Optogenetic Array Connected to the PCB and in (b) where the Connections from the Arduino (green arrow) to the Potentiometer (red arrow) and the Optogenetic Array (yellow arrow) can be seen clearly

Initially the measurement was performed in a room without considering the effect of airflow and ventilation on the measurements. This resulted in temperature variations with no relation to increase or decrease in the applied voltage or the duty cycle. Thus, to stimulate the environment of a temperature and airflow controlled room to a certain extent, a box lined with aluminium foil on the inside was used for the experiment. The experimental setup is shown in Figure 4.12.
The measurements were then made with a handheld IR thermal scanner (Fluke 63 IR Thermometer) inside this setup. Voltage and duty cycle were varied and measurements were made such that for each voltage and duty cycle ten measurements were carried out. An average of these ten measurements was used to note the temperature increase. A graph showing temperature variation for different duty cycles and applied voltage is given in Figure 4.13. The temperature shows a clear increase between different applied voltages but the variation in duty cycles also contribute heavily to the rise in temperature. The increment in duty cycles contribute to a higher increase in the accumulation of temperature for the same voltages, that is, the temperature increase at 3.4 V at 10% duty cycle (0.4°C) is much less than the temperature increase at 90% duty cycle (1.2°C) for the same applied voltage.
This pattern of behaviour is similar to results explored in Ji et al. [21] where the duty cycle and the frequency were varied at different voltages to measure the temperature variations. Although the temperature increase noted in that work varied up to 2 K, the temperature increase observed here ranges only up to 1.2°C (1.2 K). The difference in the measured maximum temperature could result from difference in experimental setups where the other work suspended the μLED array in air during measurement while the setup here places the

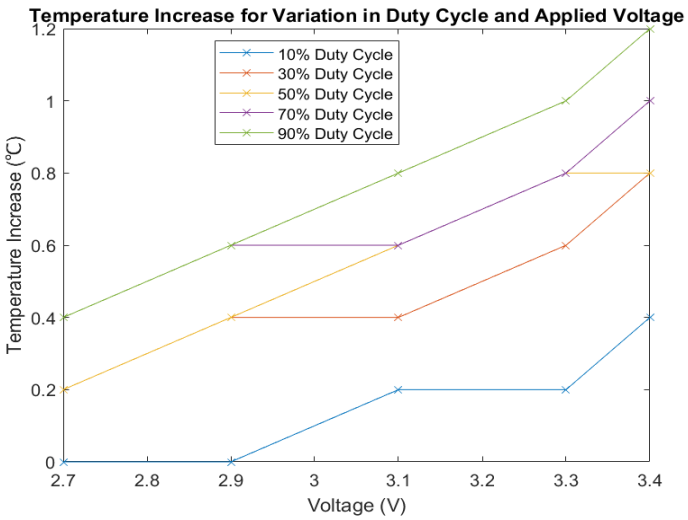

Figure 4.13: Graph depicting temperature increase with increase in applied voltage and duty cycle

μLED array on the floor of the box. However, as long as the measured temperature increase is not sustained above 0.5°C, the likelihood of tissue damage is unlikely [10]. In Figure 4.14, a temperature increase up to 0.5°C is shown to only introduce changes in cell excitability, but a sustained 1°C indicates a possibility of the blood brain barrier breakdown (BBB).

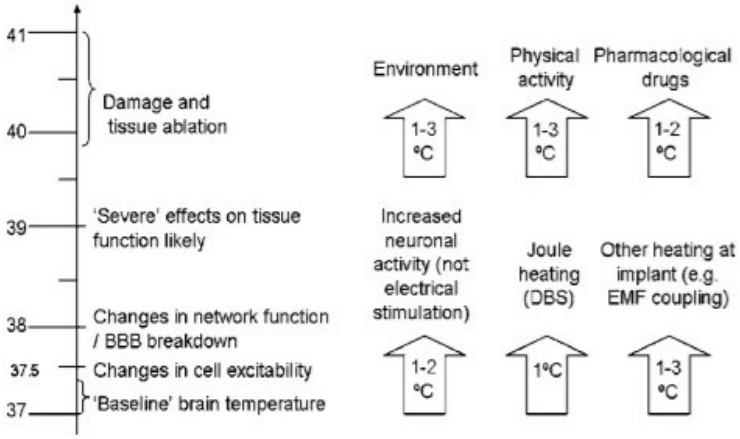

Figure 4.14: Tissue responses to temperature increase (Left) and heating factors that cause temperature increase (Right) [10]

The measured temperature increase at 2.7 V even at 90% of the duty cycle does not increase above 0.4°C in the thin film optogenetic array. However, to be on the safe side, a 2.7 V at 30% duty cycle can be used to drive the μLED array such that adequate stimulation is available to excite the neurons.

4.5. Placement of Optogenetic Array on Mouse Cortex

The thin film optogenetic array was designed with the goal of stimulating and recording responses from the cortex of a mouse's brain. So, the first objective was to determine whether the initial samples fit on the available space on the cortex. The array was fitted on the cortex of an already deceased mouse that was killed after use in a separate experiment performed at the Erasmus MC, for which official permission through the necessary channels in The Netherlands was obtained.

The array was designed to occupy an area of 6 mm X 5 mm on the cortex as discussed in 3.1.1 Shape and Space of Optogenetic Array. As already observed in 4.1.3 Lasering of Glass and PI, the problems faced with lasering the PI too close to the array resulted in damaged interconnects and unusable samples. Therefore,

3 mm of space was provided on all the sides of the array to protect the array during lasering of the PI. This overall increase in the area as shown in Figure 4.15 proved troublesome when trying to place the array on the cortex of the mouse.

Figure 4.15: Device Design with Space Consideration for Lasering of PI

This extra PI around the array was easily cut using a stainless steel blade which resulted in an optogenetic implant as shown in Figure 4.16.

Figure 4.16: Final Shape of Array Before Placement on Mouse Cortex

The array was then placed on this opening where it fit exactly. An image of the array on the mouse's cortex is shown in Figure 4.17.

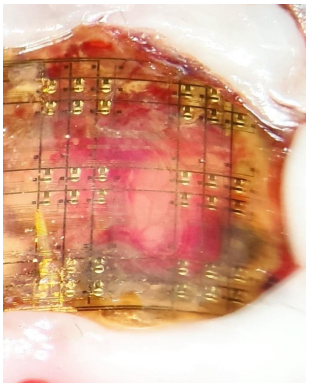

Figure 4.17: Thin Film Optogenetic Array Placed on the Cortex of a dead Mouse. Disclaimer: The array was fitted on the cortex of an already deceased mouse that was killed after use in a separate experiment performed at the Erasmus MC, for which official permission through the necessary channels in The Netherlands was obtained.

One of the main challenges during fabrication was the irregular topography introduced due to the 50 μm thickness of the μLEDs shown in Figure 4.18. This irregularity could have resulted in electrodes that are unable to make proper contact with surface of the cortex thereby leading to poor or no signals recorded after stimulation.

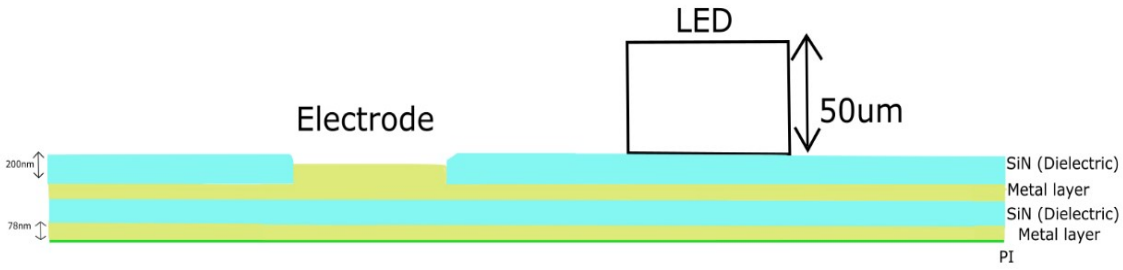

Figure 4.18: Irregular Topography of the Array due to the presence of 50 μm thick μLEDs

Although, by accounting for the presence of cerebrospinal fluid (CSF) which conducts the signals even when the electrodes do not make direct contact with the surface upon placement of the array on the cortex, the irregular topography did not prove to be a challenge as previously assumed. The ridges and grooves present on the cortex could also ensure contact to the electrodes as the PI of the array is very flexible once separated from the carrier glass substrate.

5

Conclusion

In this thesis, the design and fabrication of a flexible, large-area high density optogenetic ECoG array using thin film technology has been investigated.
The array was designed and realised using thin-film technology to be placed on the cortex of a mouse. The large area of the electrode array covers the entire cortex of the mouse and should help to map these neuronal pathways of responses from different regions on the brain. The electrodes as well as the μLEDs on the array were designed to have a pitch of 600 μm to increase resolution for stimulation and recording.
The ECoG array has an overall thickness of 14.5 μm. The bonding of the μLED increases the overall thickness to 64.5 μm. The implementation of multiple layers of Au/Ti separated by SiN, as explained in Section 3.2 Fabrication of Flexible Large Area Optogenetic Array, made it possible to increase the number of recording sites on the array, promoting an increase in the resolution of the array. The increase in the available space provided more stimulation sites for μLED bonding to increase the resolution of stimulation. The 36 untethered μLEDs bonded to the PI substrate allow multipoint stimulation on the entire cortex of the mouse's brain.
The fabrication process raised some issues that were addressed in Section 4.1 Microfabrication, which had to be overcome and improved upon. The RIE used to open vias on the first SiN layer utilized 900 W power for 260 seconds, leading to enlarged vias exposing the Au/Ti layer along with the PI substrate. By changing the power from 900 W to 100 W and reducing the exposure time for the following SiN layer, the required 10 μm vias were obtained. Following the complete fabrication of the array, during lasering the PI to separate the samples, a discrepancy in the laser resulted in the loss of 6 samples.
After the final μLED bonding done in PInS resulted in low yield of working μLEDs (~8.3%) (Table 4.2) on each sample, the connections (anode and cathode) were checked and found to have high resistances. Thus indicating open contacts at the ZIF connector used to drive the μLEDs.
Since the use of thin-film technology for an optogenetic implant is new, there was a need to characterise the array to identify the suitability of the process employed for a biomedical application. The envisioned device was designed for acute stimulation and recording experiments, so the tests performed were designed to evaluate the performance of the device over short time periods.
Initially, the Au/Ti electrodes on the array were characterised in Section 4.2.1 Electrochemical Impedance Spectroscopy using EIS in phosphate buffered saline (PBS) solution for a period of one week. After an increase in the impedance on the first day (6.28 kΩ at 1kHZ), the measured impedance remained relatively stable in the following days (~7 kΩ at 1 kHz). The behaviour of the passivation layer (SiN) above the Au/Ti layer was also characterised in PBS at the temperature of 37°C for a period of one week. The resulting decrease in the thickness of the SiN was observed using a profilometer (Table 4.1). An average dissolution of 7.3 nm of SiN was observed over the one week.
Since the μLEDs generate heat at the cortex-implant interface, the design of the μLEDs were optimally spaced to promote heat dissipation. The heat generated at each μLED due to different driving voltages and duty cycles also contribute to the problem. Hence, as discussed in Section 4.4 Thermal Characterisation, the μLEDs on the array were driven using an Arduino Mega at varying voltages and duty cycles. The observed increase in maximum temperature at 90% duty cycle is 1.2°C at a maximum voltage of 3.4 V, while the temperature at 10% duty cycle for the same voltage is 0.4°C. Temperature measurements suggest that the duty cycle applied to the μLED contribute more to a temperature increase as compared to the case when voltage is applied.
The use of thin-film technology contributes to the novelty of the implant as it allows fabrication of sub-micron

thicknesses of each layer on the array (substrate, interconnects, SiN, electrodes). The result was an extremely flexible optogenetic array that was finally placed on the cortex of a mouse's brain. Before placement, the extra PI used for protection purposes around the edges of the array has been cut away. The array proved to fit adequately in the open region around the skull made by a surgical incision.

6

Future Work

The findings of this work have clarified some aspects that could be improved. As mentioned in Section 3.1 of this thesis, the μLEDs used in this array had dimensions of 220 X 270 μm with a height of 50 μm. This height increased the overall thickness of the array and created an irregular topography on the array as discussed in Section 4.5. Smaller μLEDs with height of ~10 μm can be used in place instead. GaN based-μLEDs with select dimensions can be grown on sapphire or silicon substrates and transfer printed using laser lift-off to a substrate material of choice. Placement of these μLEDs can be done using a PDMS stamp if pick and place cannot be employed due to the small size.

PI was chosen as the substrate material for the optogenetic array because of its relatively low Young's Modulus and because it is used as a substrate material extensively in TFT processing in Holst Centre. Alternatively, flexible materials such as parylene-C could also be explored as substrates for an optogenetic array.

The final design of the optogenetic implant had interconnects of 70 mm length leading to a ZIF connector of 36 mm as shown in Section 3.1. The length of 70 mm was initially provided to allow for easy handling during implantation on the mouse cortex. However, the length proved too long for a mouse to move around naturally with the implant protruding from its head with the large ZIF connector attached to a PCB. The length of the routing can be reduced to ~20 to 30 mm and choice for a smaller ZIF connector can be pursued.

Apart from considering alternative materials to develop a stable optogenetic implant, detailed characterisation methods have to be established to be aware of the performance of the device. Starting with the electrodes, EIS was performed in PBS for a week at room temperature to characterise the electrodes. This only provided preliminary results and the performance of the electrodes in body temperature for at least 2 to 4 weeks would prove better insight to understand the progression of electrochemical reactions on the Au electrode surface. The same can be performed to determine the behaviour of the passivation layer (SiN) in PBS before implementing in in-vivo measurements.

The passivation material used as the final layer can also be replaced with a parylene-c or a PI layer to increase the longevity of the implant in PBS or for in-vivo measurements.

The optogenetic implant implemented here is a passive array with individually addressable μLEDs. Although an active matrix optogenetic array can be realised using the full TFT process with transistors used to drive the LEDs, there is still a need to determine the biocompatibility of the thin-film technology employed. The process used during fabrication of the array is unconventional and thus the reaction of biological tissue to the implant is still relatively unknown. By implanting the passive array for short period of time in different animal models, the anatomical and biological response of the subject can be analysed. The resolution of stimulation and recording can also be investigated during this time by driving the μLEDs while recording the responses from the cortex of the subject.

A

Arduino Code

```
int led_pin = 13;
int pot_pin = A0;
int output;
int led_value;
float voltage;
void setup() {
  Serial.begin(9600);
  pinMode(led_pin, OUTPUT);
}
void loop() {
  //Reading from potentiometer
  output = analogRead(pot_pin);
  voltage = output*(5.0/1023.0);
  //Mapping the Values between 0 to 255 because we can give output
  //from 0 -255 using the analogwrite funtion
  led_value = map(output, 0, 1023, 0, 255);
  analogWrite(led_pin, led_value);
  delay(3);
  Serial.print(voltage);
  Serial.print("\t");
  Serial.println(output);
  //loop for duty cycle of LED at 90%
  for (int i=0; i<=5000; i++){
digitalWrite(led_pin, HIGH);
delayMicroseconds(90);
digitalWrite(led_pin, LOW);
delayMicroseconds(100-90);
}
delay(1000);
}
```

Bibliography

[1] Suleman Ayub, Luc J. Gentet, Richárd Fiáth, Michael Schwaerzle, Mélodie Borel, François David, Péter Barthó, István Ulbert, Oliver Paul, and Patrick Ruther. Hybrid intracerebral probe with integrated bare led chips for optogenetic studies. Biomedical Microdevices, 19, 9 2017. ISSN 1387-2176. doi: 10.1007/s10544-017-0190-3.

[2] Satarupa Biswas, Debdeep Sikdar, Debanjan Das, Manjunatha Mahadevappa, and Soumen Das. Pdms based multielectrode arrays for superior in-vitro retinal stimulation and recording. Biomedical Microdevices, 19, 12 2017. ISSN 1387-2176. doi: 10.1007/s10544-017-0221-0.

[3] Johan Bobacka, Andrzej Lewenstam, and Ari Ivaska. Electrochemical impedance spectroscopy of oxidized poly(3,4-ethylenedioxythiophene) film electrodes in aqueous solutions. Journal of Electroanalytical Chemistry, 489:17–27, 7 2000. ISSN 1572-6657. doi: 10.1016/S0022-0728(00)00206-0.

[4] Christian Boehler, Stefano Carli, Luciano Fadiga, Thomas Stieglitz, and Maria Asplund. Tutorial: guidelines for standardized performance tests for electrodes intended for neural interfaces and bioelectronics. Nature Protocols, 15, 11 2020. ISSN 1754-2189. doi: 10.1038/s41596-020-0389-2.

[5] Jonathan P. Britt, Ross A. McDevitt, and Antonello Bonci. Use of channelrhodopsin for activation of cns neurons. Current Protocols in Neuroscience, 58, 1 2012. ISSN 1934-8584. doi: 10.1002/0471142301.ns0216s58.

[6] E Cheng, Ben Xing, Shanshan Li, Chengzhuang Yu, Junwei Li, Chunyang Wei, and Cheng Cheng. Pressure-driven micro-casting for electrode fabrication and its applications in wear grain detections. Materials, 12, 11 2019. ISSN 1996-1944. doi: 10.3390/ma12223710.

[7] A. Das, A. Sinha, V.R. Rao, and K.N. Jonnalagadda. Fracture in microscale su-8 polymer thin films. Experimental Mechanics, 57, 6 2017. ISSN 0014-4851. doi: 10.1007/s11340-017-0262-6.

[8] Karl Deisseroth. Optogenetics. Nature Methods, 8, 1 2011. ISSN 1548-7091. doi: 10.1038/nmeth.f.324.

[9] David Ding, Yichen Lu, Ruoyu Zhao, Xin Liu, Chawina De-Eknamkul, Chi Ren, Armaghan Mehrsa, Takaki Komiyama, and Duygu Kuzum. Evaluation of durability of transparent graphene electrodes fabricated on different flexible substrates for chronic in vivo experiments. IEEE Transactions on Biomedical Engineering, 67, 11 2020. ISSN 0018-9294. doi: 10.1109/TBME.2020.2979475.

[10] Maged M. Elwassif, Qingjun Kong, Maribel Vazquez, and Marom Bikson. Bio-heat transfer model of deep brain stimulation induced temperature changes. IEEE, 8 2006. ISBN 1-4244-0032-5. doi: 10.1109/IEMBS.2006.259425.

[11] Vasiliki Giagka and Wouter A. Serdijn. Realizing flexible bioelectronic medicines for accessing the peripheral nerves – technology considerations. Bioelectronic Medicine, 4, 12 2018. ISSN 2332-8886. doi: 10.1186/s42234-018-0010-y.

[12] R A Green, P B Matteucci, C W D Dodds, J Palmer, W F Dueck, R T Hassarati, P J Byrnes-Preston, N H Lovell, and G J Suaning. Laser patterning of platinum electrodes for safe neurostimulation. Journal of Neural Engineering, 11, 10 2014. ISSN 1741-2560. doi: 10.1088/1741-2560/11/5/056017.

[13] Seth A Hara, Brian J Kim, Jonathan T W Kuo, Curtis D Lee, Ellis Meng, and Victor Pikov. Long-term stability of intracortical recordings using perforated and arrayed parylene sheath electrodes. Journal of Neural Engineering, 13, 12 2016. ISSN 1741-2560. doi: 10.1088/1741-2560/13/6/066020.

[14] Jennifer Hay. Measuring substrate-independent young's modulus of thin films, 2011.

[15] Klaus-Peter Hoffmann, Roman Ruff, and Wigand Poppendieck. Long-term characterization of electrode materials for surface electrodes in biopotential recording. IEEE, 8 2006. ISBN 1-4244-0032-5. doi: 10.1109/IEMBS.2006.260443.

[16] M.M.R. Howlader, T.E. Doyle, S. Mohtashami, and J.R. Kish. Charge transfer and stability of implantable electrodes on flexible substrate. Sensors and Actuators B: Chemical, 178, 3 2013. ISSN 09254005. doi: 10.1016/j.snb.2012.12.051.

[17] T. i. Kim, J. G. McCall, Y. H. Jung, X. Huang, E. R. Siuda, Y. Li, J. Song, Y. M. Song, H. A. Pao, R.-H. Kim, C. Lu, S. D. Lee, I.-S. Song, G. Shin, R. Al-Hasani, S. Kim, M. P. Tan, Y. Huang, F. G. Omenetto, J. A. Rogers, and M. R. Bruchas. Injectable, cellular-scale optoelectronics with applications for wireless optogenetics. Science, 340, 4 2013. ISSN 0036-8075. doi: 10.1126/science.1232437.

[18] Jae Woong Jeong, Jordan G. McCall, Gunchul Shin, Yihui Zhang, Ream Al-Hasani, Minku Kim, Shuo Li, Joo Yong Sim, Kyung In Jang, Yan Shi, Daniel Y. Hong, Yuhao Liu, Gavin P. Schmitz, Li Xia, Zhubin He, Paul Gamble, Wilson Z. Ray, Yonggang Huang, Michael R. Bruchas, and John A. Rogers. Wireless optofluidic systems for programmable in vivo pharmacology and optogenetics. Cell, 162:662–674, 7 2015. ISSN 0092-8674. doi: 10.1016/J.CELL.2015.06.058.

[19] Jinmo Jeong, Namsun Chou, and Sohee Kim. Long-term characterization of neural electrodes based on parylene-caulked polydimethylsiloxane substrate. Biomedical Microdevices, 18, 6 2016. ISSN 1387-2176. doi: 10.1007/s10544-016-0065-z.

[20] Y. S. Jeong, B. Ratier, A. Moliton, and L. Guyard. Uv–visible and infrared characterization of poly(p-xylylene) films for waveguide applications and oled encapsulation. Synthetic Metals, 127:189–193, 3 2002. ISSN 0379-6779. doi: 10.1016/S0379-6779(01)00621-X.

[21] Bowen Ji, Zhejun Guo, Minghao Wang, Bin Yang, Xiaolin Wang, Wen Li, and Jingquan Liu. Flexible polyimide-based hybrid opto-electric neural interface with 16 channels of micro-leds and electrodes. Microsystems Nanoengineering, 4, 12 2018. ISSN 2055-7434. doi: 10.1038/s41378-018-0027-0.

[22] Angelique C. Johnson and Kensall D. Wise. An active thin-film cochlear electrode array with monolithic backing and curl. Journal of Microelectromechanical Systems, 23, 4 2014. ISSN 1057-7157. doi: 10.1109/JMEMS.2013.2288947.

[23] Dongmin Kim, Tomoyuki Yokota, Toshiki Suzuki, Sunghoon Lee, Taeseong Woo, Wakako Yukita, Mari Koizumi, Yutaro Tachibana, Hiromu Yawo, Hiroshi Onodera, Masaki Sekino, and Takao Someya. Ultra-flexible organic light-emitting diodes for optogenetic nerve stimulation. Proceedings of the National Academy of Sciences, 117, 9 2020. ISSN 0027-8424. doi: 10.1073/pnas.2007395117.

[24] Thomas Knopfel and Edward S Boyden. Optogenetics: tools for controlling and monitoring neuronal activity. Elsevier, 2012.

[25] Ki Yong Kwon, B. Sirowatka, Wen Li, and A. Weber. Opto-microecog array: Transparent microecog electrode array and integrated leds for optogenetics. IEEE, 11 2012. ISBN 978-1-4673-2293-5. doi: 10.1109/BioCAS.2012.6418471.

[26] Ki Yong Kwon, Brenton Sirowatka, Arthur Weber, and Wen Li. Opto-ecog array: A hybrid neural interface with transparent ecog electrode array and integrated leds for optogenetics. IEEE Transactions on Biomedical Circuits and Systems, 7, 10 2013. ISSN 1932-4545. doi: 10.1109/TBCAS.2013.2282318.

[27] Nicolò Lago and Andrea Cester. Flexible and organic neural interfaces: A review. Applied Sciences, 7, 12 2017. ISSN 2076-3417. doi: 10.3390/app7121292.

[28] Mikhail A. Lebedev and Miguel A.L. Nicolelis. Brain-machine interfaces: past, present and future, 9 2006. ISSN 01662236.

[29] Yichen Lu, Xin Liu, Ryoma Hattori, Chi Ren, Xingwang Zhang, Takaki Komiyama, and Duygu Kuzum. Ultralow impedance graphene microelectrodes with high optical transparency for simultaneous deep two-photon imaging in transgenic mice. Advanced Functional Materials, 28, 8 2018. ISSN 1616301X. doi: 10.1002/adfm.201800002.

[30] J C Lötters, W Olthuis, P H Veltink, and P Bergveld. The mechanical properties of the rubber elastic polymer polydimethylsiloxane for sensor applications. Journal of Micromechanics and Microengineering, 7, 9 1997. ISSN 0960-1317. doi: 10.1088/0960-1317/7/3/017.

[31] Niall McAlinden, Erdan Gu, Martin D. Dawson, Shuzo Sakata, and Keith Mathieson. Optogenetic activation of neocortical neurons in vivo with a sapphire-based micro-scale led probe. Frontiers in Neural Circuits, 9, 5 2015. ISSN 1662-5110. doi: 10.3389/fncir.2015.00025.

[32] Eve McGlynn, Vahid Nabaei, Elisa Ren, Gabriel Galeote-Checa, Rupam Das, Giulia Curia, and Hadi Heidari. The future of neuroscience: Flexible and wireless implantable neural electronics. Advanced Science, 8, 5 2021. ISSN 2198-3844. doi: 10.1002/advs.202002693.

[33] Jerrold S Meyer and Linda F Quenzer. Psychopharmacology: Drugs, the brain, and behavior. Sinauer Associates, 2005. ISBN 0-87893-534-7 (Hardcover).

[34] Sami Myllymaa, Katja Myllymaa, and Reijo Lappalainen. Flexible implantable thin film neural electrodes. InTech, 10 2009. ISBN 978-953-307-004-9.

[35] DIETER OESTERHELT and WALTHER STOECKENIUS. Rhodopsin-like protein from the purple membrane of halobacterium halobium. Nature New Biology, 233, 9 1971. ISSN 0090-0028. doi: 10.1038/newbio233149a0.

[36] Weihua Pei and Hongda Chen. Electrode array for neural interfaces, 2018.

[37] C. J. Robin, Aakansha Vishnoi, and Krishna N. Jonnalagadda. Mechanical behavior and anisotropy of spin-coated su-8 thin films for mems. Journal of Microelectromechanical Systems, 23, 2 2014. ISSN 1057-7157. doi: 10.1109/JMEMS.2013.2264341.

[38] P.J. Rousche, D.S. Pellinen, D.P. Pivin, J.C. Williams, R.J. Vetter, and D.R. Kipke. Flexible polyimide-based intracortical electrode arrays with bioactive capability. IEEE Transactions on Biomedical Engineering, 48, 3 2001. ISSN 0018-9294. doi: 10.1109/10.914800.

[39] Krishna Seshan. Deposition technologies and applications: Introduction and overview, 2002.

[40] Joseph T. Smith, Barry O'Brien, Yong-Kyun Lee, Edward J. Bawolek, and Jennifer Blain Christen. Application of flexible oled display technology for electro-optical stimulation and/or silencing of neural activity. Journal of Display Technology, 10, 6 2014. ISSN 1551-319X. doi: 10.1109/JDT.2014.2308436.

[41] Enming Song, Hui Fang, Xin Jin, Jianing Zhao, Chunsheng Jiang, Ki Jun Yu, Yiding Zhong, Dong Xu, Jinghua Li, Guanhua Fang, Haina Du, Jize Zhang, Jeong Min Park, Yonggang Huang, Muhammad A. Alam, Yongfeng Mei, and John A. Rogers. Thin, transferred layers of silicon dioxide and silicon nitride as water and ion barriers for implantable flexible electronic systems. Advanced Electronic Materials, 3:1–8, 2017. ISSN 2199160X. doi: 10.1002/aelm.201700077.

[42] Soeren Steudel, Jan-Laurens P.J. van der Steen, Manoj Nag, Tung Huei Ke, Steve Smout, Thijs Bel, Karin van Diesen, Gerard de Haas, Joris Maas, Joris de Riet, Madelon Rovers, Roy Verbeek, Yen-Yu Huang, Shin-Chuan Chiang, Marc Ameys, Florian De Roose, Wim Dehaene, Jan Genoe, Paul Heremans, Gerwin Gelinck, and Auke Jisk Kronemeijer. Power saving through state retention in igzo-tft amoled displays for wearable applications. Journal of the Society for Information Display, 25, 4 2017. ISSN 10710922. doi: 10.1002/jsid.544.

[43] Thomas Stieglitz. Flexible biomedical microdevices with double-sided electrode arrangements for neural applications. Sensors and Actuators A: Physical, 90:203–211, 5 2001. ISSN 0924-4247. doi: 10.1016/S0924-4247(01)00520-9.

[44] Zeike Taylor and Karol Miller. Reassessment of brain elasticity for analysis of biomechanisms of hydrocephalus. Journal of Biomechanics, 37:1263–1269, 8 2004. ISSN 0021-9290. doi: 10.1016/J.JBIOMECH.2003.11.027.

[45] Jinbi Tian, Zexu Lin, Zhiyuan Chen, Sofian N. Obaid, Igor R. Efimov, and Luyao Lu. Stretchable and transparent metal nanowire microelectrodes for simultaneous electrophysiology and optogenetics applications. Photonics, 8, 6 2021. ISSN 2304-6732. doi: 10.3390/photonics8060220.

[46] Andrada Iulia Velea, Sten Vollebregt, Tim Hosman, Anna Pak, and Vasiliki Giagka. Towards a microfabricated flexible graphene-based active implant for tissue monitoring during optogenetic spinal cord stimulation. IEEE, 10 2019. ISBN 978-1-7281-2637-1. doi: 10.1109/NMDC47361.2019.9084021.

[47] Jonathan Viventi, Dae Hyeong Kim, Leif Vigeland, Eric S Frechette, Justin A. Blanco, Yun Soung Kim, Andrew E Avrin, Vineet R Tiruvadi, Suk Won Hwang, Ann C. Vanleer, Drausin F Wulsin, Kathryn Davis, Casey E Gelber, Larry Palmer, Jan Van Der Spiegel, Jian Wu, Jianliang Xiao, Yonggang Huang, Diego Contreras, John A. Rogers, and Brian Litt. Flexible, foldable, actively multiplexed, high-density electrode array for mapping brain activity in vivo. Nature Neuroscience, 14:1599–1605, 2011. ISSN 10976256. doi: 10.1038/nn.2973.

[48] Fan Wu, Eran Stark, Pei-Cheng Ku, Kensall D. Wise, György Buzsáki, and Euisik Yoon. Monolithically integrated leds on silicon neural probes for high-resolution optogenetic studies in behaving animals. Neuron, 88, 12 2015. ISSN 08966273. doi: 10.1016/j.neuron.2015.10.032.

[49] S. Yamagiwa, M. Ishida, and T. Kawano. Flexible optrode array: Parylene-film waveguide arrays with microelectrodes for optogenetics. IEEE, 6 2015. ISBN 978-1-4799-8955-3. doi: 10.1109/TRANSDUCERS.2015.7180915.

[50] Dóra Zelena, Kornél Demeter, József Haller, and Diána Balázsfi. Considerations for the use of virally delivered genetic tools for in-vivo circuit analysis and behavior in mutant mice: a practical guide to optogenetics. Behavioural Pharmacology, 28, 12 2017. ISSN 0955-8810. doi: 10.1097/FBP.0000000000000361.

[51] Feng Zhang, Li-Ping Wang, Martin Brauner, Jana F. Liewald, Kenneth Kay, Natalie Watzke, Phillip G. Wood, Ernst Bamberg, Georg Nagel, Alexander Gottschalk, and Karl Deisseroth. Multimodal fast optical interrogation of neural circuitry. Nature, 446, 4 2007. ISSN 0028-0836. doi: 10.1038/nature05744.

[52] Zhengtuo Zhao, Lan Luan, Xiaoling Wei, Hanlin Zhu, Xue Li, Shengqing Lin, Jennifer J. Siegel, Raymond A. Chitwood, and Chong Xie. Nanoelectronic coating enabled versatile multifunctional neural probes. Nano Letters, 17, 8 2017. ISSN 1530-6984. doi: 10.1021/acs.nanolett.7b00956.

[53] Tao Zhou, Guosong Hong, Tian-Ming Fu, Xiao Yang, Thomas G. Schuhmann, Robert D. Viveros, and Charles M. Lieber. Syringe-injectable mesh electronics integrate seamlessly with minimal chronic immune response in the brain. Proceedings of the National Academy of Sciences, 114, 6 2017. ISSN 0027-8424. doi: 10.1073/pnas.1705509114.